ORNL/TM-2015/59349

ORNL Evaluation of Electrabel Safety Cases for Doel 3 / Tihange 2: Final Report (R2)

ORNL
B. Richard Bass
Terry L. Dickson
Sarma B. Gorti
Hilda B. Klasky
Randy K. Nanstad
Mikhail A. Sokolov
Paul T. Williams

ATI Consulting
William L. Server

November 2015

OAK RIDGE NATIONAL LABORATORY
MANAGED BY UT-BATTELLE FOR THE US DEPARTMENT OF ENERGY

ORNL/TM-2015/59349

Computational Sciences and Engineering Division

ORNL EVALUATION OF ELECTRABEL SAFETY CASES FOR DOEL 3 / TIHANGE 2: FINAL REPORT (R2)

ORNL
B. Richard Bass
Terry L. Dickson
Sarma B. Gorti
Hilda B. Klasky
Randy K. Nanstad
Mikhail A. Sokolov
Paul T. Williams

ATI Consulting
William L. Server

Date Published: November 2015

Prepared by
OAK RIDGE NATIONAL LABORATORY
Oak Ridge, Tennessee 37831-6283
managed by
UT-BATTELLE, LLC
for the
US DEPARTMENT OF ENERGY
under contract DE-AC05-00OR22725

CONTENTS

Page

LIST OF FIGURES

Figure **Page**

LIST OF TABLES

Table **Page**

ACRONYMS

AFCN	Agence fédérale de contrôle nucléaire – Belgian Federal Agency for Nuclear Control
ASME	American Society of Mechanical Engineers
ASTM	American Society for Testing and Materials (ASTM International since 2001)
BPVC	ASME Boiler and Pressure Vessel Code
D3/T2	Doel 3 and Tihange 2
EBL	Electrabel, ENGIE Group
EPFM	elastic-plastic fracture mechanics
FANC	Federaal Agentschap voor Nucleaire Controle – Belgian Federal Agency for Nuclear Control
FAVOR	Fracture Analysis of Vessels – Oak Ridge
IRB	International Review Board
LEFM	linear-elastic fracture mechanics
LOCA	Loss of Coolant Accident
ORNL	Oak Ridge National Laboratory, Oak Ridge, TN, USA (USDOE National Laboratory)
RPV	Reactor Pressure Vessel
RSE-M	Règles de Surveillance en Exploitation des Matérials Mécaniques des Illots Nucléaires French code providing Rules for Inservice Inspection of Nuclear Power Plant Components
SIA	Structural Integrity Assessment
USDOE	United States Department of Energy
USNRC	United States Nuclear Regulatory Commission
UT	ultrasonic testing
WPS	warm-prestress
XFEM	eXtended Finite Element Method

Revision History		
Version Number	***Description of Changes***	***Issue Date***
R0	Initial Issue	November 12, 2015
R1	Minor editorial revisions (no results or conclusions were affected)	November 13, 2015
R2	Minor format revisions (no results or conclusions were affected)	December 08, 2015

NOMENCLATURE

Greeks

α_x, α_y	inclination angles for box in Fig. 5.1; tilt = $\max\left(\alpha_x, \alpha_y\right)$
ν	Poisson's ratio

Variables

$2a$	diameter of circular flaw in Figs. 5.2 and 5.3
$2a_{cc}$	acceptable flaw size
ΔK	cyclical change in stress intensity factor for fatigue crack growth analysis
G	energy release rate for an LEFM crack
G_{eq}	energy release rate for an LEFM crack under mixed-mode loading
K_I	Mode I LEFM stress intensity factor for crack face opening loading
K_{II}	Mode II LEFM stress intensity factor for in-plane shear loading
K_{III}	Mode III LEFM stress intensity factor for out-of-plane shear loading
K_{Ia}	crack arrest fracture toughness
K_{Ic}	plane strain fracture toughness
K_{eq}	mixed-mode stress intensity factor representing equivalent energy release rate, G_{eq}
K_{IR}	crack growth resistance fracture toughness
L_x, L_y	box diagonals in Fig. 5.1
P	pressure
RT_{NDT}	reference temperature for nil-ductility transition
SF	safety factor
S	ligament length in Fig. 5.1
T	temperature
t	time
T_o	Master Curve material reference temperature from ASTM E1921-15[1]
T_{41J}	Charpy index temperature at 41 Joules absorbed impact energy from ASTM A370-14[2]

[1] ASTM Standard E1921, 2015,: *Standard Test Method for Determination of Reference Temperature, T_0, for Ferritic Steels in the Transition Range,* ASTM International, West Conshohocken, PA.

[2] ASTM Standard A370, 2014, *Standard Test Methods and Definitions for Mechanical Testing of Steel Products,* ASTM International, West Conshohocken, PA

ABSTRACT

Oak Ridge National Laboratory (ORNL) performed a detailed technical review of the 2015 Electrabel (EBL) Safety Cases prepared for the Belgium reactor pressure vessels (RPVs) at Doel 3 and Tihange 2 (D3/T2). The Federal Agency for Nuclear Control (FANC) in Belgium commissioned ORNL to provide a thorough assessment of the existing safety margins against cracking of the RPVs due to the presence of almost laminar flaws found in each RPV. Initial efforts focused on surveying relevant literature that provided necessary background knowledge on the issues related to the quasi-laminar flaws observed in D3/T2 reactors. Next, ORNL proceeded to develop an independent quantitative assessment of the entire flaw population in the two Belgian reactors according to the American Society of Mechanical Engineers (ASME) Boiler and Pressure Vessel Code, Section XI, Appendix G, "Fracture Toughness Criteria for Protection Against Failure," New York (1992 and 2004). That screening assessment of all EBL-characterized flaws in D3/T2 used ORNL tools, methodologies, and the ASME Code Case N-848, "Alternative Characterization Rules for Quasi-Laminar Flaws". Results and conclusions from the ORNL flaw acceptance assessments of D3/T2 were compared with those from the 2015 EBL Safety Cases. Specific findings of the ORNL evaluation of that part of the EBL structural integrity assessment focusing on stability of the flaw population subjected to primary design transients include the following:

- ORNL's analysis results were similar to those of EBL in that very few characterized flaws were found not compliant with the ASME (1992) acceptance criterion.
- ORNL's application of the more recent ASME Section XI (2004) produced only four non-compliant flaws, all due to LOCAs.
- The finding of a greater number of non-compliant flaws in the EBL screening assessment is due principally to a significantly more restrictive (conservative) criterion for flaw size acceptance used by EBL.
- ORNL's screening assessment results (obtained using an analysis methodology different from that of EBL) are interpreted herein as confirming the EBL screening results for D3/T2.
- ORNL's independent refined analysis demonstrated the EBL-characterized flaw 1660, which is non-compliant in the ORNL and EBL screening assessment, is rendered compliant when modeled as a more realistic individual quasi-laminar flaw using a 3-D XFEM analysis approach.
- ORNL's and EBL's refined analyses are in good agreement for the flaw 1660 close to the clad/base metal interface; ORNL is not persuaded that repeating this exercise for more than one non-compliant flaw is necessary to accept the EBL conclusions derived from the aggregate of EBL refined analysis results.

ORNL General Conclusions Regarding the Structural Integrity Assessment (SIA) Conducted by EBL for D3/T2 – Based on comparative evaluations of ORNL and EBL SIA analyses and on consideration of other results, ORNL is in agreement with the general conclusions reported by Electrabel in their RPV D3/T2 Technical Summary Note of April 14, 2015:

- More than 99 percent of flaws in D3/T2 meet the defined screening criterion, rendering them benign with respect to initiation in the event of a design transient.
- Refined analyses of non-compliant flaws from the screening assessment indicate that only 11 of the 16196 detected flaws have a critical reference-temperature material index (designated RT_{NDT}) that implies the possibility of the initiation of cleavage fracture at some future time. For those 11

flaws, the calculated margin in RT_{NDT} (a measure of acceptable embrittlement relative to end-of-service-life conditions) is significant, being greater than 80 °C.

- Fatigue crack growth is not a concern in the flaw-acceptability analyses.
- Primary stress re-evaluation confirms that the collapse pressure is more than 1.5 times the design pressure in the presence of defects detected in D3/T2.
- Sufficient conservatisms are built into the input data and into the different steps of the SIA; in some cases, those conservatisms are quantified and imply that additional margins exist in the SIA.
- Taken as a whole, the foregoing results and conclusions confirm the structural integrity of Doel 3 and Tihange 2 under all design transients with ample margin in the presence of the 16196 detected flaws.

1. INTRODUCTION AND BACKGROUND

During a scheduled outage of the Doel 3 and Tihange 2 (D3/T2) units in Summer of 2012, an ultrasonic inspection of a new kind revealed a large number of flaw indications in the lower and upper core shells of the RPVs. Short-term actions were performed by the licensee as requested and the Nuclear Safety Regulator, the FANC, gave the go-ahead to restart both units in May 2013. However, in March 2014, one of the mid-term actions led to unexpected results. As a result, the licensee decided that both reactors had to be shut down again. This action was related to the mechanical properties of a flaked material under irradiation and it appeared that the material embrittlement was greater than expected. Now, before allowing a potential restart of the D3/T2 reactors, the FANC is expecting the licensee EBL to reassess its safety case. Owing to the technical and scientific complexity of the issue and its impact on the safety of both units, the FANC decided that its safety review process for both reactors should exceptionally include an independent review by an external research team. ORNL was selected by the FANC for this work due to its nearly 50-year history (still ongoing) of research and development in the area of RPVs for the U.S. Nuclear Regulatory Commission (USNRC) and for the U.S. Department of Energy (USDOE).

Expectations of the FANC for the ORNL review are outlined in the form of an overall objective that includes seven tasks as described in *Chapter 2* of this report. It is specifically noted that the structural integrity calculations in Subtask 7 were requested by the FANC and represent the greatest portion of this report.

2. OBJECTIVES

The overall objective of this assessment is to provide a critical review of the safety cases for the D3/T2 reactors, i.e., a thorough assessment of the existing safety margins against cracking in the RPVs as a result of deterioration due to the presence of almost laminar flaws in the wall of each RPV. Critical elements of the safety demonstration submitted by the licensee EBL are covered by this project, excluding the qualification of the ultrasonic instrument and the non-destructive examinations.

2.1 SUBTASKS

The detailed objectives specified by the FANC are shown herein as subtasks, 1 through 7, with the title of each subtask in the exact wording provided by the FANC.

1. Assess the acceptability of each assumption considered by the licensee in the safety case except for the qualification of the ultrasonic instrument and the non-destructive examinations.

2. Assess the safety margins and the level of conservatism for the successive steps of the approach submitted by the licensee.

3. Identify any non-standard aspects for a safety justification of a nuclear RPV.

4. Identify the new techniques developed by the licensee.

5. Assess the acceptability of these non-standard aspects and new techniques in the successive steps of the justification of the structural integrity of the RPVs.

6. Identify:

    6.1. The mistakes,
    6.2. The questionable and unjustified aspects, and
    6.3. The questionable and justifiable – though lightly justified and documented – aspects in the safety case.

7. If requested by the FANC, perform structural integrity calculations with the same input parameters used by the licensee to verify the analysis presented in the Safety Case and compare the results with those in the Safety Case.

2.2 DELIVERABLES

The following deliverables were completed during the tenure of this project:

- ***One month after approval to start work, ORNL provided weekly email messages to the FANC regarding progress in reading the provided documents.***
- ***Seven weeks following start of formal review of the Safety Case:*** During week 8 of the Safety Case review, ORNL prepared and submitted to the FANC an Intermediate Report of the Safety Case review. That intermediate report (submitted to the FANC on November 5, 2015) provided an overview of the main points of the review outcome and primary background information needed for clarification of those main points. Also, that report included in *Section* 5.0 a quantification of acceptance of the detected flaw population in the two Belgian reactors according to the ASME Boiler and Pressure Vessel Code, Section XI (1992 and 2004).

- ***Two weeks following FANC review of the Intermediate Report:*** In the case of no further information, supplements or corrections to the Intermediate Report, ORNL will submit a final formal report to the FANC; this document is the initial version of that final report. If the FANC requests additional review, completion of such additional work will be determined through negotiation.

3. TECHNICAL PREPARATORY DOCUMENT REVIEW

3.1 OBJECTIVE

Technical documents provided by the FANC were reviewed by team members in general accordance with document relevance to the team member's expertise and responsibility within the project; e.g., material properties of unirradiated and irradiated materials and microstructural evaluations, relevant test standards and codes, e.g., ASME Boiler and Pressure Vessel Code (BPVC), structural integrity analysis, application of structural integrity calculation codes, etc.

3.2 APPROACH

Initial efforts were focused on surveying relevant literature that provided necessary background knowledge on the issues related to the quasi-laminar flaws observed in the D3/T2 reactors in Belgium.

3.3 RESULTS

The ORNL review team notes that the EBL project for the D3/T2 RPVs represents a very robust and comprehensive analysis to investigate the effects of quasi-laminar flaws on structural integrity, and is even more noteworthy given the very high quality and quantity of their work in a relatively short period of time. We have found exhaustive documentation backed by robust tests and computational analyses that have contributed to the development of science and engineering in this field.

4. ASSESSMENT OF MATERIAL PROPERTIES

Structural integrity analysis (SIA) of Doel 3 and Tihange 2 reactor pressure vessels is the primary focus of this project, but the material properties of the reactor vessels are parameters directly used in the SIA and are briefly discussed in this chapter. The information presented in this chapter was gleaned from the documents provided to ORNL for this project by the FANC, with specific references provided in each section as appropriate.

4.1 HYDROGEN FLAKES EFFECT ON MECHANICAL PROPERTIES, ESPECIALLY FRACTURE TOUGHNESS

A large experimental program has been executed to address the potential effects of hydrogen flakes on mechanical properties and, especially, fracture toughness [1-3]. Three types of forgings were used by Electrabel to evaluate and characterize the effect of hydrogen flakes on mechanical properties. First, examination of the cut-offs from the upper core and nozzle shells of the D3 and T2 forgings was very obvious and well justified. However, only the nozzle shells have segregated areas and, moreover, these segregated areas are associated with "ghost lines" and no hydrogen flakes were identified. Thus, the addition of two other forgings with a high density of hydrogen flakes is considered a critical aspect of the entire testing program. These two forgings, VB395 and KS02, are somewhat different from the D3/T2 forgings. They have different manufacturing histories, chemical compositions, etc., and both of them were known to have flakes.

Three types of mechanical tests have been used to characterize potential effects of hydrogen flakes on mechanical properties – tensile, Charpy V-notch instrumented impact, and fracture toughness tests, thus covering all major types of mechanical testing. For fracture toughness testing, both precracked Charpy bend bar (PCCV) and 12.5-mm thick compact tension (CT12.5) specimens were used.

The main observation from this work can be summarized as follows: *tests performed on flaked material (VB395 and KS02 forgings) show that the presence of flakes has no substantial impact on the mechanical properties as very similar results were obtained for specimens with flakes, for specimens taken between flakes, and for specimens taken outside the flaked area.* The test program demonstrated that there is a similar effect of segregation on initial RT_{NDT}, T_{41J}, and T_0 for D3/T2 and VB395 forgings under non-irradiated conditions. For the KS02 forging, the effect is somewhat larger as described in the following section. In addition, tests on the D3H1 nozzle shell cut-out showed that ghost lines have practically no effect on Charpy impact and fracture toughness properties. In particular, for the VB395 forging, no significant difference in T_0 was observed between CT12.5 specimens taken between flakes and CT12.5 specimens with real flakes as pre-cracks, demonstrating that the presence of hydrogen flakes has no effect on the material properties.

4.2 CHARPY V-NOTCH IMPACT DATA COMPARED WITH FRACTURE TOUGHNESS DATA

The mechanical testing on different materials under non-irradiated conditions showed that in the transition region there is no significant effect of the specimen orientation or segregation level on the Charpy V-notch and fracture toughness properties [1-3]. For the D3/T2 RPV forgings, the differences in T_{41J} between segregated and non-segregated zones are 22 °C and 6 °C for the T2H2 and D3H1 nozzle shell cut-outs, respectively. In a similar way, fracture toughness tests showed that the effect of segregations on the initial T_0 was less than 10°C for both cut-outs. For the KS02 flange forging, the difference in T_{41J} between segregated and non-segregated areas is 47 °C, i.e., larger than in the D3/T2 forgings and VB395. The difference in T_0 between both areas is 25 °C, i.e., larger than in the D3/T2 forgings, but similar to VB395. For the VB395 forging, the difference in Master Curve T_0 encountered in different material zones in Block 6 (specimens with flakes, taken between flakes or adjacent to the flaked

area) is less than 25 °C. In terms of RT_{NDT} (T_{41J}), this difference is less than 20 °C. Overall, the differences between fracture toughness T_0 and Charpy V-notch T_{41J} measured on all tested materials in the unirradiated condition are within the scatter band observed on various RPV steels.

4.3 SURVEILLANCE DATA FOR DOEL 3 AND TIHANGE 2

Both Doel 3 [2] and Tihange 2 [3] surveillance programs contained specimens from upper core shell forgings. In the surveillance program, only material from the non-segregated areas was included. Figure 4.1 presents the shift of T_{41J} vs fluence as well as results of the supplemental irradiation experiment CHIVAS-10. Surveillance data are designated as D3 and T2. Both surveillance programs, D3 and T2, cover a fluence range in excess of 6.0×10^{19} n/cm^2 (E>1MeV) which is considered as the fluence corresponding to 40 years of operation. The surveillance data from D3 and T2 demonstrate very good correspondence between the measured T_{41J} shifts and the predictions by the French RSE-M[3] predictive equation.

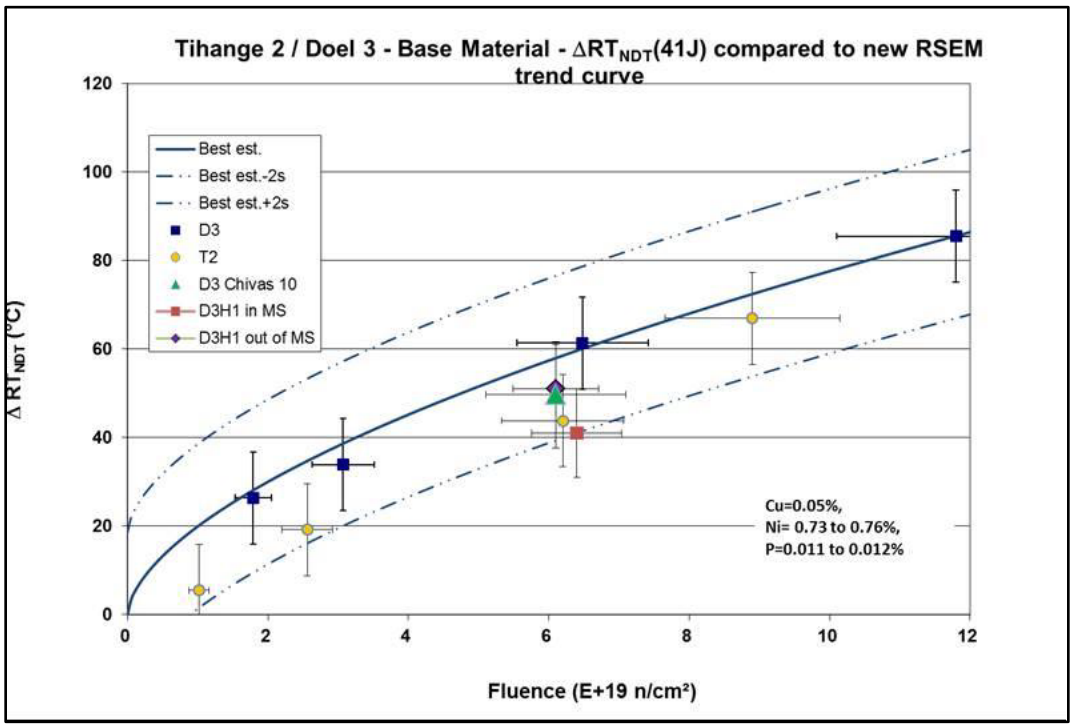

Fig. 4.1 Comparison of Doel 3 and Tihange 2 surveillance program data with RSE-M prediction and with CHIVAS-10 data.

4.4 IRRADIATION EXPERIMENTS WITH VB395 AND KS02

In addition to the reactor surveillance data available for both D3 and T2, a series of irradiation experiments were conducted in the BR-2 test reactor at SCK-CEN with the D3 nozzle shell cut-out, the D3 upper core shell, the KS02 flange, and the VB395 shell. Charpy V-notch impact, tensile, and fracture toughness specimens were irradiated so that data are available at various neutron fluences from about 1 to 12×10^{19} n/cm^2 (>1 MeV), depending on the specific material [1-3]. The surveillance data and the BR-2

[3] Règles de Surveillance en Exploitation des Matérials Mécaniques des Illots Nucléaires (RSE-M) is a French code that provides Rules for Inservice Inspection of Nuclear Power Plant Components.

data for the D3/T2 materials (see Fig. 4.1 for example) and for the KS02 forging behave in general accordance with the applicable French RSE-M irradiation predictive model. For the KS02 flaked material, the data are within the predicted scatter and near the two-sigma upper bound of the RSE-M prediction; that is not necessarily surprising since the nickel content for KS02 is greater than that in the predictive model and higher nickel is known to increase radiation sensitivity in RPV steels. For the VB395 forging, however, the irradiation behavior of that material has demonstrated very disparate radiation sensitivities, depending on which toughness test and which region of the forging the specimens are taken from. The fracture toughness Master Curve reference temperature shifts, ΔT_0, multiplied by a commonly used correlation between Charpy impact transition temperature and fracture toughness shift, are well above the RSE-M predictive model for both material in the flaked regions and material out of the flaked regions. On the other hand, the Charpy impact shift data are within the bounds of the predictive model for out-of-flake specimens but well above the predictive model bounds for the between-flakes specimens. The material also exhibited a substantial degree of additional embrittlement, which appears to be abnormal non-hardening embrittlement, the root cause (see *Section* 4.6) for which has not yet been determined even with an international expert panel assessment. Additionally, a separate part of the VB395 forging, designated Block 5, exhibited very disparate behavior in that the ΔT_0 was extremely low even at the relatively high fluence of 2×10^{19} n/cm^2, and then showed very rapid increase in ΔT_0 with increasing fluence at the same rate of increase shown by the specimens in the out-of-flakes and in the between-flakes regions. Furthermore, the Block 5 material exhibited irradiation-induced hardening in accordance with the relevant predictive model. These very disparate results point to an extremely inhomogeneous material leading to the observation, as discussed in *Section 4.1*, that the primary benefit from the testing of this material is that the hydrogen flakes did not substantially affect the fracture toughness of the material.

4.5 RELEVANCE OF VB395 AND KS02 TO D3/T2

The forging VB395 was fabricated for an AREVA steam generator shell according to the French specification for 18MND5 steel which is similar to the ASME specification SA 508 class 3, both being in the class of MnMoNi steels. Although the ladle chemical analyses for VB395 and D3/T2 are generally very similar, the analyses revealed that the chrome contents for the D3/T2 vessel forgings ranged from 0.04 to 0.18 wt%, while that of VB395 is significantly higher at 0.254 wt% [2,3]. The VB395 forging shell was discovered to have a relatively high density of hydrogen flakes and was rejected prior to being put into service. The forging was obtained by Electrabel as a surrogate for the D3/T2 materials to enable mechanical property and irradiation effects research on a material with a high density of hydrogen flakes. The manufacturing processes for VB395 involved forging of a hollow ingot without piercing and, apparently, heat treatment with an inadequate de-hydrogenation procedure, resulting in thousands of hydrogen flakes and significant macro-segregation primarily in the central portions of the shell walls, with the hydrogen flakes being located within micro-segregated areas designated ghost lines. Although both the D3/T2 and VB395 materials are largely bainitic, the VB395 material contains more tempered martensite with a concomitant higher overall hardness. A major observation of properties in the unirradiated condition is that similar test results are obtained for specimens with flakes, for specimens taken between flakes and taken outside the flaked areas.

The KS02 forged flange was manufactured in Germany according to specification 20MnMoNi55, also similar to ASME SA 508 class 3 steel [2,3]. In this material, however, the ladle analysis shows that the manganese is somewhat lower, while the chrome and nickel are significantly higher than for the D3/T2 forgings. The KS02 forging was manufactured with a solid ingot but with no piercing and was also discovered to have a high density of hydrogen flakes in the central portion of the thickness. The relatively recent availability of material from the KS02 forging provided a second surrogate material with which to assess mechanical properties and irradiation effects of a material with a large number of hydrogen flakes. This forging was substantially thicker than the D3/T2 vessel forgings and the VB395 forging. The microstructure of KS02 is a mix of lower and upper bainite with some tempered martensite similar to the D3/T2 materials and with similar hardness.

The relevance of both VB395 and KS02 to the D3/T2 forgings lies in the fact that they contain substantial numbers of hydrogen flakes making them microstructurally similar to the specific D3/T2 forgings which contain hydrogen flakes. They have somewhat similar chemical compositions in that they were fabricated to similar low-alloy specifications for reactor pressure vessel steels, but there are differences relative to radiation sensitivities, especially in the case of VB395 as mentioned above. As stated earlier, our opinion is that the VB395 and KS02 materials are relevant to D3/T2 primarily with regard to the fact that they contain high densities of hydrogen flakes which is valuable in assessing if the hydrogen flakes have significant effects on the mechanical properties and fracture toughness of the D3/T2 forgings as a consequence of exposure to irradiation. The fact that Electrabel has applied an additional margin based on the behavior of the irradiated VB395 material is considered an additional conservatism.

4.6 ROOT CAUSE OF EXCESSIVE EMBRITTLEMENT OF VB395

The root cause for the abnormal and excessive embrittlement of the VB395 forging is not thoroughly known. Electrabel has done some extensive work to assess the root cause, but the exact mechanism(s) are not clearly defined at this time [2,3]. Two mechanisms are considered plausible especially since they relate to the unusual fabrication history associated with VB395. These two possible mechanisms are the segregation of impurities such as phosphorus to carbides or precipitation interfaces in the matrix and loss of strength due to the higher levels of martensite which may produce abnormal embrittlement. Neither of these mechanisms can be easily proven, but the fact that the fabrication history was abnormal leading to higher levels of chromium from the contaminated ladle and the different heat treatment suggest that VB395 is not typical of the forgings in Doel 3 or Tihange 2. The German KS02 material also had hydrogen flakes and did not exhibit abnormal embrittlement due to irradiation. Therefore, ORNL suggests that further research be conducted to discern the exact mechanism(s), but because of the fact that the embrittlement applied for the Doel 3 and Tihange 2 vessels uses the enhanced embrittlement as determined for the VB395 material, the predictions of toughness change due to irradiation are considered conservative.

4.7 MARGIN CALCULATIONS

The overall margin calculations for material fracture toughness shift behavior due to irradiation in terms of a final RT_{NDT} value were reviewed. The fairly recent evaluation by Electrabel [4] in response to additional questions was very comprehensive and added new clarity. The International Review Board (IRB) had suggested that the margin for the initial RT_{NDT}, reflective of the highly segregated area, may not be adequate, but the overall margin using the VB395 penalty covered this area of uncertainty. The recent calculations from Electrabel delved into detail on this topic and, using a new approach to the overall margin needed, showed that the current method has other built-in margins that should compensate for this area of concern. ORNL is in agreement with the appropriately conservative margin applied by Electrabel in the Safety Cases [2,3].

4.8 CONCLUSIONS FOR MATERIALS PROPERTIES ASSESSMENT

- Tests performed on flaked material (VB395 and KS02 forgings) show that the presence of flakes has no substantial impact on the mechanical properties as very similar results were obtained for specimens with flakes, for specimens taken between flakes, and for specimens taken outside the flaked area.
- Overall, the differences between the Master Curve fracture toughness index temperature, T_0 , and Charpy V-notch index temperature at 41 Joules absorbed impact energy, T_{41J} , measured on all tested materials in the unirradiated condition are within the scatter band observed on various RPV steels.
- The surveillance data from D3 and T2 demonstrate very good correspondence between the measured T_{41J} shifts and the predictions by the French RSE-M predictive equation.

- Regarding the VB395 forging, very disparate results point to an extremely inhomogeneous material leading to the observation that the primary benefit from the testing of this material is that the hydrogen flakes did not substantially affect the fracture toughness of the material.
- The VB395 and KS02 materials are only relevant to D3/T2 primarily with regard to the fact that they each contain a high density of hydrogen flakes that is valuable in assessing if the hydrogen flakes have significant effects on the mechanical properties and fracture toughness of the D3/T2 forgings as a consequence of exposure to irradiation. The fact that Electrabel has applied an additional margin based on the behavior of the irradiated VB395 material is considered an additional conservatism.
- The root cause for the abnormal and excessive embrittlement of the VB395 forging is not thoroughly known at this time. Although not necessary for application to D3/T2, ORNL suggests that further research be conducted to discern the exact mechanism(s) of the abnormal embrittlement to provide additional knowledge regarding behavior of forgings with hydrogen flakes.
- A concern expressed by the International Review Board regarding the margin applied to the unirradiated RT_{NDT} for the D3/T2 materials resulted in Electrabel using a new approach to the overall margin, with recent calculations showing that the current method has other built-in margins that compensate for this area of concern. ORNL is in agreement with the appropriately conservative margin applied by Electrabel in the Safety Cases.

5. EVALUATION OF ELECTRABEL STRUCTURAL INTEGRITY ASSESSMENTS OF DOEL 3 AND TIHANGE 2 RPVS

5.1 INTRODUCTION

According to ref. [1], EBL performed an SIA to

> "verify that the structural integrity of the RPV is maintained under all operating conditions given the presence of detected flaws. The SIA was performed for all relevant loading conditions according to the applicable rules of the ASME Boiler & Pressure Vessel Code. As such, it includes
>
> - Assessment of the absence of crack initiation for all individual flaws with adequate safety margins,
> - Assessment of the stability of the flaws through fatigue crack growth evaluation, and
> - Satisfaction of the primary stress intensity acceptance criteria.

This section provides an ORNL evaluation of the foregoing elements of the EBL SIA performed for D3/T2. In that evaluation, ORNL gave priority to the first element of that SIA, i.e., the EBL assessment of existing margins against crack initiation for the full population of flaws found in D3/T2. Specifically, ORNL performed extensive computational analyses to produce an independent quantitative assessment of the detected flaw population in D3/T2 according to the ASME Boiler and Pressure Vessel Code, Section XI, Appedix G, "Fracture Toughness Criteria for Protection Against Failure," New York (1992 and 2004) [5-6]; conclusions regarding the EBL flaw assessment methodology were then drawn based on comparisons of ORNL and EBL results. For the other two elements of the EBL SIA, i.e., flaw stability with respect to fatigue crack growth and primary stress intensity acceptance, ORNL provided an evaluation of the EBL results/conclusions, but did not perform independent analyses due to time constraints on ORNL participation.

5.2 APPROACH

The primary work scope for this task directs ORNL to

- perform structural integrity calculations using the same input parameters employed by EBL to verify the flaw assessment analysis in the EBL safety case, and to
- compare results with those in the EBL safety case.

Stringent time constraints placed on completion of that work scope has restricted ORNL to actually performing only selected elements of the EBL SIA. The approach taken by ORNL is to focus on analysis elements of the EBL SIA that

(1) are judged to be critical to the safety case, and

(2) can be executed by ORNL in the allotted time frame.

Specifically, ORNL has taken the following steps:

- reviewed the EBL flaw screening assessment of D3/T2 that is based on the ASME Section XI (1992) [5] criterion;
- performed an independent screening assessment of all EBL-characterized flaws in D3/T2 using ORNL tools, methodologies, and ASME Section XI criteria/code case;
- performed some limited refined analyses of those characterized flaws NOT satisfying ASME Section XI acceptance criteria;
- compared ORNL results and conclusions regarding flaw acceptance assessment of D3/T2 with those from the EBL safety case.

Completion of the foregoing work scope is described in the following sections/discussions that

- summarize the specific parts of the SIA performed by EBL that relate to the brittle-fracture stability of the flaw population in D3/T2 subjected to screened design transients. A review of the EBL flaw assessment procedure herein is essential because the ORNL flaw assessment of D3/T2 uses much of that EBL methodology;
- describe the ORNL procedure for performing the screening analyses of the entire EBL-characterized flaw population to identify those flaws that violate ASME acceptance criteria when subjected to the screened design transients;
- present and discuss ORNL results obtained from application of ASME Section XI (both 1992 and 2004) to the EBL-characterized flaw population in D3/T2;
- compare ORNL and EBL results from flaw screening studies, particularly for characterized flaws that do NOT satisfy ASME flaw acceptance criteria;
- describe ORNL results from refined analyses of a characterized individual flaw that failed the acceptance criteria; the latter involves ABAQUS eXtended Finite Element Method (XFEM) analyses of the flaws using techniques similar to those employed by EBL;
- assess results of the EBL methodologies that were applied to

  (1) screening assessments of characterized flaws, and to

  (2) refined analyses of those characterized flaws that fail the screening criteria;
- provide evaluations regarding two additional elements of the EBL SIA, i.e., flaw stability with respect to fatigue crack growth and primary stress intensity acceptance; (ORNL did not perform independent analyses to support those evaluations).

5.3 SUMMARY OF EBL SIA FLAW ACCEPTANCE ASSESSMENT

For convenience of the reader, this section summarizes input data, methodology, results and conclusions from the EBL SIA that are deemed essential to the ORNL evaluation; those selections are drawn primarily from ref. [1].

5.3.1 Input Data

Input data for the EBL SIA were drawn from refs. [2 – 3] and include the following:

- RPV geometry,
- updated UT measurements on the “flakes” or quasi-laminar defects,
- load (pressure, temperature, film heat transfer coefficient) versus time transients taken from the design transient file, and
- material properties.

Reference [7] provides additional details concerning the EBL SIA input.

5.3.2 Flaw Acceptability Assessment

The SIA reported by EBL was carried out in accordance with the *ASME Section XI (1992) Rules for Inservice Inspection of Nuclear Power Plant Components* [5]. That assessment included characterizing every flaw based on dimensional data gathered via ultrasonic measurements and subjecting each characterized flaw to a specified design transient loading. The flaw characterization process is summarized in the steps given below.

5.3.3 Flaw Modeling

5.3.3.1 Individual Flaws

Each individual flaw is characterized by a "three-dimensional box" that completely envelops the flaw (See Fig. 5.1). The characterized flaw is then defined by the geometric parameters representing the box: the diagonals, L_x, L_y, of the faces of the box; the tilt (inclination) (α_x, α_y) of the diagonals; S is the minimum distance from the box to the clad/base interface. In that box, the largest possible flaw is the elliptical configuration (dotted line) shown in Fig. 5.2. Introducing an additional level of conservatism, EBL applied the actual acceptability assessment to the solid circle in Fig. 5.2 that envelops the ellipse.

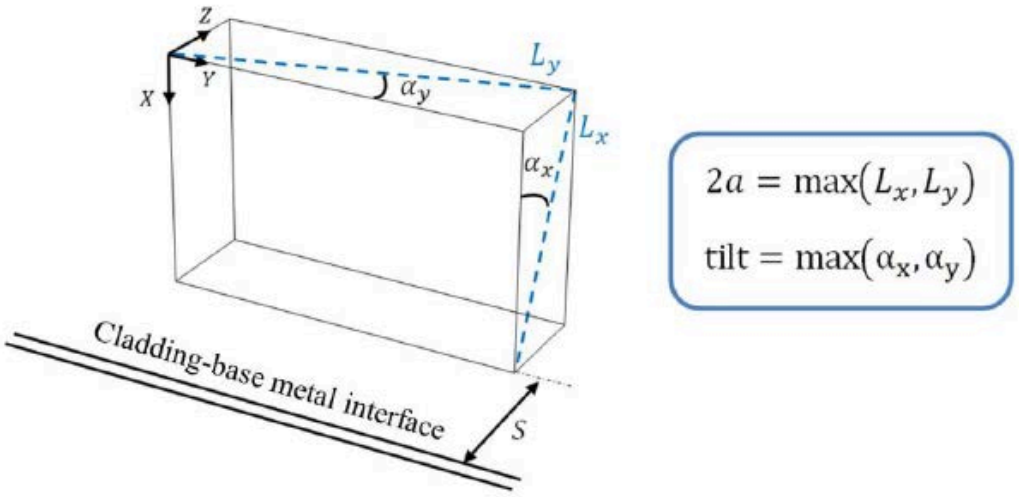

Fig. 5.1 Geometric parameters defining the characterized flaw (see Fig. 3.5.3 in Ref. [1]).

Thus, the characterization of the individual quasi-laminar flaw is defined by the following parameters:

- flaw size, i.e., diameter of the enveloping circle (the larger of L_x, L_y),
- ligament S, i.e., the shortest distance from the 3-D box to the clad-base metal interface, and
- tilt, i.e., inclination of the plane of the circle with respect to the inner surface of the vessel [the larger of (α_x, α_y) but limited to 20 ° for individual flaws based on ultrasonic data].

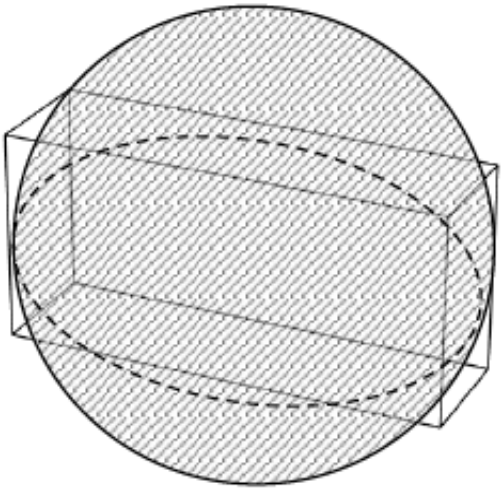

Fig. 5.2 Characterization of flaw by a circle that envelops the largest possible elliptical flaw (see Fig. 3.5.4 in ref. [1]).

5.3.3.2 Grouping of Closely Spaced (Interacting) Flaws

EBL developed specific grouping rules for closely spaced flaws using 3-D finite element modeling and experimental data [8]. These grouping rules were applied to all possible pairs of flaws to determine whether or not two or more flaws satisfy established interaction rules [9-10] that require they be grouped into one single flaw. In Fig. 5.3, the grouping rule is depicted schematically for three flaws that are grouped into a single box [see Fig. 5.3(a)]. A single circular flaw [see Fig. 5.3(b)] encompassing the three grouped flaws is defined in the same manner as for the individual flaw, with the exception that the 20 degree limitation on tilt for individual flaws is not applied to the group circular flaw. Thus, the flaw size (i.e., diameter) of the enveloping circular flaw can be much larger than each of the individual flaws in the grouping box.

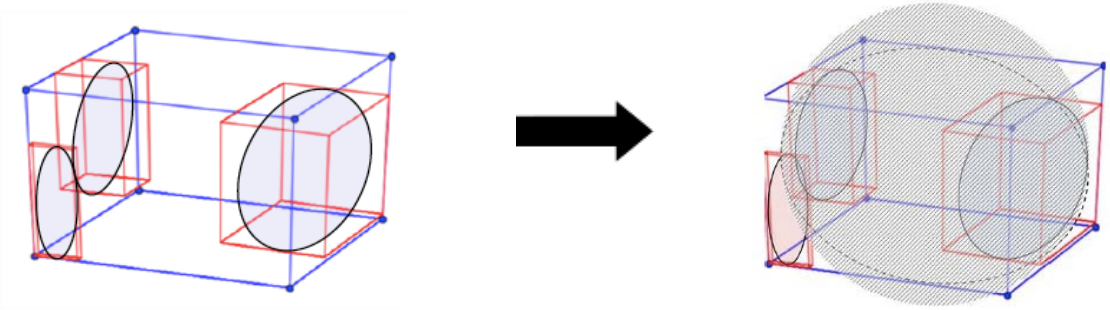

(a) (b)

Fig. 5.3 Grouping of three closely-spaced interacting flaws into a single, independent, circular flaw (see Fig. 3.5.5 -3.5.6 in ref.[1])

5.3.4 Transient Loading – Pressure and Temperature

EBL screened the primary system design transients to determine those that are most severe (for cleavage fracture) with respect to position of the quasi-laminar flaw in the RPV wall as measured by ligament *S* (Refs. [11-12]). Results of that screening reported by EBL are given as follows (see Fig. 5.4):

- 0-20 mm – loss of coolant accidents (LOCAs),
- 20-30 mm – cool-down transients, and
- > 30 mm – heat-up transients.

The screened design transients include the following:

- Doel 3 – one transient each for cool-down, heat-up and LOCA, and
- Tihange 2 – one transient each for cool-down and heat-up; two LOCA transients, i.e., one small-break and one large-break.

Plots of pressure, *P*, and coolant temperature, *T* , versus time, *t* , for the five design transients provided by EBL (ref. [7]) are shown in Figs. B.1 – B.5 of Appendix B to this report.

The EBL screening analysis performed for each of the characterized flaws (single and grouped) was based on selection of a particular design transient for assessing that flaw according to the following constraints:

- plant-specific design transients (recall that Doel 3 has one LOCA, while Tihange 2 has two LOCAs),
- ligament *S*, and
- transient/ligament binning defined above and depicted in Fig. 5.4.

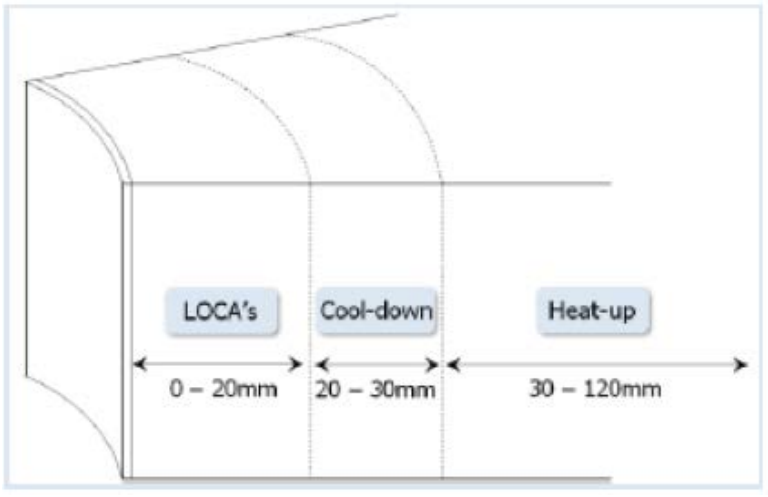

Fig. 5.4 Classification of driving transient for EBL-characterized flaws according to ligament length *S* (see Fig 5.1 (Fig. 3.5.7 in ref.[1]).

5.3.5 Acceptance Criterion for Flaw Size

EBL used the ASME XI Code (1992) acceptance criterion (see ref. [5]) to determine acceptable flaw size for the characterized flaw population in D3/T2. That criterion is given as follows:

$$K_I(2a) < \frac{K_{IR}}{SF} \tag{5.1}$$

where

$2a$ = diameter of circular flaw in Fig. 5.2 and Fig. 5.3,
K_I = applied stress-intensity factor,
K_{IR} = fracture toughness crack growth resistance,
SF = Safety Factor $\left(\sqrt{2} \text{ or } \sqrt{10}\right)$,
$K_{IR} = K_{Ia}$; $SF = \sqrt{10}$ for level A/B transients (cool-down and heat-up),
$K_{IR} = K_{Ic}$; $SF = \sqrt{2}$ for level C/D transients (LOCAs),
K_{Ia} = fracture arrest toughness, and
K_{Ic} = plane strain fracture toughness.

EBL used 3-D finite element analysis to construct flaw acceptance curves for the tilted circular flaws (Fig. 5.2-Fig. 5.3) subjected to the screened driving transients (see Fig. 5.4) according to the flaw characterizing parameters

- ligament S,
- flaw tilt angle, and
- RT_{NDT} – reference temperature for nil-ductility transition.

5.3.6 Flaw Screening Criterion

According to ref. [1], EBL screened both individual and grouped flaws according to the criterion

$$2a < \left(0.5 \times 2a_{acc}\right) \tag{5.2}$$

where

$2\ a_{acc}$ = acceptable flaw size for a given set of parameters defined in the foregoing section.

A high percentage of the characterized flaws in D3/T2 satisfied that screening criterion (refs. [13-14]). As shown in Fig. 5.5, a total of 28 flaws in Doel 3 and 9 flaws in Tihange 2 did not satisfy the criterion; a tabular listing of those non-compliant flaws is included in *Section* 5.6 of this report. EBL addressed that finding by subjecting all non-compliant flaws to more refined analyses as described below.

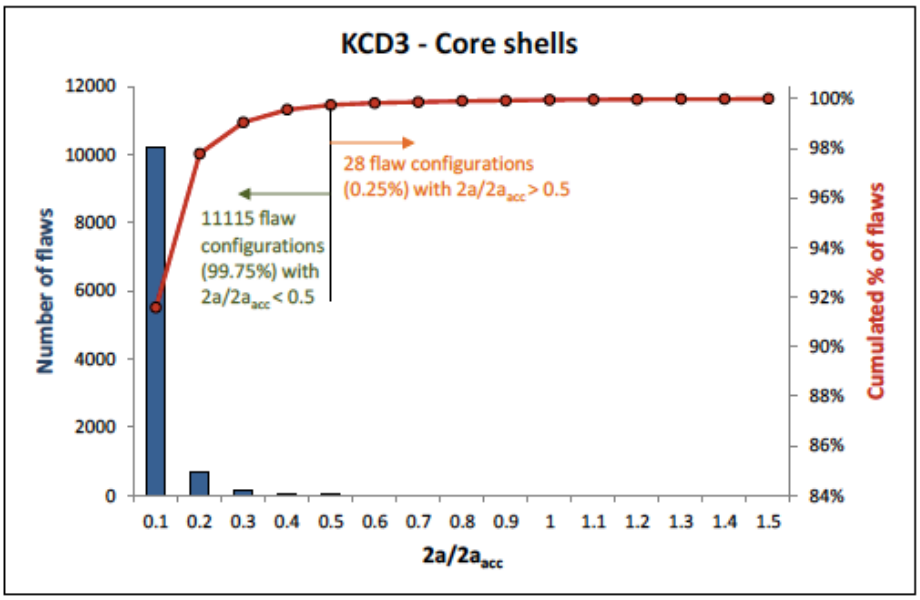

(a)

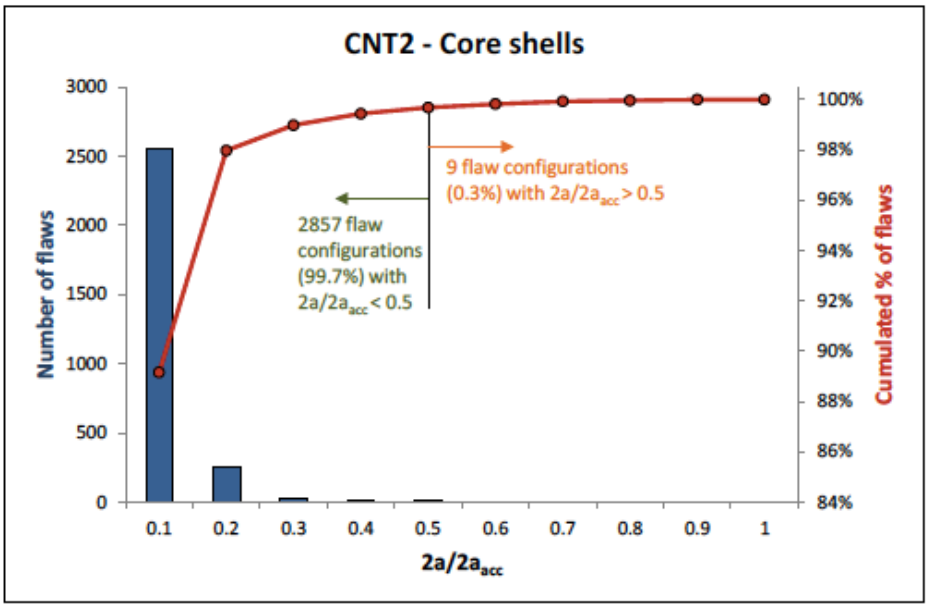

(b)

Fig. 5.5 Application of EBL flaw screening criterion to D3/T2 (a) Doel 3 and (b) Tihange 2 (Figs 3.5.9 and 3.5.10 in ref.[1]).

5.3.7 Refined Analyses of Characterized Flaws not Compliant with Screening Criterion

Refined analyses performed by EBL (ref. [1]) on those characterized flaws not compliant with the EBL screening criterion incorporate two changes from the foregoing screening analyses:

- Flaws are modeled as ellipses fitting into the rectangular 3-D-boxes (see Fig. 5.6), rather than as larger tilted circles;
- Flaws previously in a group are no longer part of a group, but are modeled individually in a multi-flaw model that accounts for mechanical interactions among closely spaced flaws.

Three-dimensional eXtended Finite Element Method (XFEM) analyses were performed on those refined flaw characterizations using the unaltered inputs from the screening analyses. All flaws subjected to the refined analyses were reported to have met the acceptance criterion with ample margin (ref.[1]); some specific details are listed in the following section.

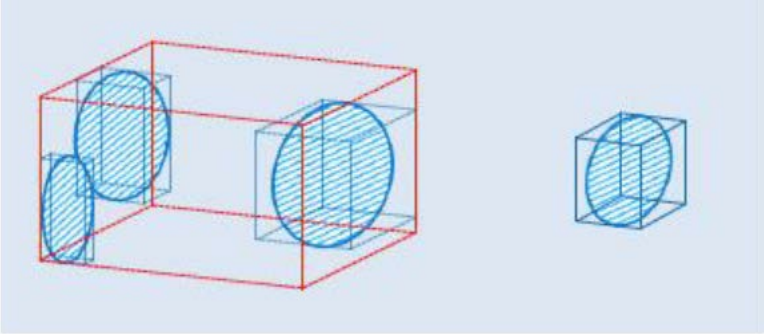

Fig. 5.6 EBL refined analyses use a more realistic flaw characterization, in which flaws are modeled as ellipses contained in 3-D boxes (see Fig. 3.5.11 in ref. [1]).

5.3.8 Conclusions of the Flaw Acceptance Assessment

The EBL structural integrity assessment confirmed (among other results) the absence of crack initiation for all individual flaws. Specifically,

- more than 99 percent of Doel 3 and Tihange 2 flaws satisfy the screening criterion, $2a < \left(0.5 \times 2a_{acc}\right)$;
- for the remaining flaws not satisfying the screening criterion, refined analyses show that the maximum crack driving force is well below the fracture toughness lower shelf, $K_{IR,lower\ shelf}$ (i.e., without an *SF*);
- for the 11 remaining flaws having a maximum crack driving force that exceeds $K_{IR,lower\ shelf}/SF$, the calculated margin in RT_{NDT} is large, more than 80 °C (see ref.[1]).

5.4 EBL FATIGUE CRACK GROWTH ANALYSES

Fatigue crack growth analyses [15-16] were performed by EBL using analytical procedures given in ASME Section XI, Appendix A, "Analysis of Flaws." The stated objective of those analyses was to

assess stability of the quasi-laminar flaws with respect to fatigue crack growth through end of service life. A conservative approach was defined and executed in several steps:

- Characterized flaws were distributed in subcategories defined in terms of flaw tilt.
- Reference flaws covering maximum size and minimum ligament were determined for each subcategory.
- Reference flaws were projected onto the axial plane.
- ΔK was calculated from ASME Section XI Appendix A using solutions for elliptical flaws subjected to design transient loading.
- Fatigue crack growth calculation formula was derived from ASME Section XI Appendix A rate curve and occurrences of design transient loading.

Analysis results predicted maximum flaw growth over entire service life of 3.19 % for Doel 3 and 1.66 % for Tihange 2. EBL concluded that fatigue crack growth is not a concern in the flaw acceptance analyses.

5.5 EBL ASME SECTION III PRIMARY STRESS RE-EVALUATION

EBL performed a primary stress re-evaluation [17-18] as prescribed by ASME Section III "Rules for Construction of Nuclear Facility Components." That evaluation accounted for the existing flaw population in D3/T2 and was performed to verify that the calculated collapse pressure should be more than 1.5 times the design pressure. The re-evaluation was performed in the following steps:

- The RPV wall was screened slice-by-slice to determine the region with highest flaw density.
- The region of highest flaw density was reconstructed with a 2-D finite element model.
- An elastic-plastic finite element analysis was performed to determine the collapse pressure according to ASME Section III Code Article NB-3228.3 and to verify the primary stress limits.
- The collapse pressure was determined to be more than 1.5 times the design pressure.

5.6 ORNL FLAW ACCEPTANCE ASSESSMENT OF D3/T2 RPVS

ORNL performed a SIA of D3/T2 RPVs for the purpose of confirming selected results and conclusions reported by EBL in refs. [1-3]. The ORNL analyses were focused on the following elements:

- flaw acceptance assessments based on ASME Section XI criteria (versions 1992 and 2004); and
- refined analyses of a selected characterized flaw not compliant with the ASME Section XI acceptance criteria.

Generally, the ORNL approach to the SIA of D3/T2 follows the sequence of steps taken by the EBL assessment as summarized in the previous sections. However, there are several specific differences in the ORNL approach that will be identified and explained in the description below. Two of those differences are the following:

- The FAVOR, v12.1 code[4] is used to compute crack driving forces, i.e., applied stress intensity factors (K_I), at the flaw tip in applications of the acceptance criteria; by contrast, EBL employed XFEM methodology and 3-D finite element models to perform those computations.

[4] Minor modifications were made to FAVOR, v12.1, to accommodate the specific format of the EBL-provided flaw input data.

- The ASME Code Case N-848 [19] was used to generate a variant of the EBL characterization of the quasi-laminar flaw population to render the latter compatible with the FAVOR v12.1 code; a detailed description of the ORNL approach is presented below.

5.6.1 Input Data

The ORNL analyses used the RPV geometries, flaw characterization files, pressure and temperature versus time transients, and material properties provided by EBL as listed above in *Section 5.3.1*. Reference [7] provides comprehensive details concerning the EBL SIA input data that were conveyed to ORNL for this report.

5.6.2 Flaw Modeling

Application of the FAVOR code [20] to assessments of the quasi-laminar flaw population in D3/T2 requires a flaw characterization that meets the following requirements:

- axial and/or circumferential flaws normal to principal stress directions of the RPV that are amenable to Mode I fracture mechanics analysis,
- for embedded (non-surface) flaws, the configuration must be fully elliptical, and
- flaws are assumed mechanically independent, i.e., flaws do not interact.

The effects of proximity/flaw interaction and flaw orientation were examined in two recent papers [9-10] and translated into the ASME Code Case N-848 [19]. Those documents provide suitable rules to incorporate flaw interaction and orientation effects for quasi-laminar and planar flaws based on their alignment and distance between them.

Specifically, ASME Code Case N-848 [19] defines the characterization of quasi-laminar and planar flaws. A bounding box is defined for

- an individual flaw,
- a grouped flaw (two or more quasi-laminar flaws), or
- an extended combined flaw (containing also a planar flaw).

In *Section* 5 of [19], that bounding box (containing a single flaw or grouped flaws) is resolved into two rectangular planar flaws corresponding to the faces of the box normal to the principal stresses. The two planar flaws

- are normal to the principal stress directions,
- retain the surface/subsurface characterization defined for a combined flaw,
- assume the dimensions of the relevant surfaces of the bounding box, and
- have no interaction.

As described previously, the D3/T2 flaw characterization files conveyed to ORNL by EBL (ref. [7]) include the full population of indications in bounding boxes containing individual or grouped flaws that are treated as non-interacting; thus, the EBL characterization files are compatible with *Section* 5 of the ASME code case. The next step to render the characterization files acceptable to FAVOR is to resolve each bounding box listed in the input file into two elliptical planar flaws corresponding to the faces of the box normal to the principal stresses, as depicted in Fig. 5.7. Two criteria are used to define the major and minor axes of each ellipse:

- the major axes of the ellipse are in the same ratio as the sides of the rectangle, and
- the area of the ellipse is the same as the area of the corresponding rectangle.

FAVOR employs relevant ASME code methodology [21] to compute applied K_I (crack driving forces) at the elliptical flaw tip as a function of the opening-mode stress field generated by a specified transient loading.

Thus, the re-generated flaw characterization file that is input to FAVOR contains two elliptical flaws for each of the boxed flaws appearing in the original EBL characterization file. Additional details concerning the foregoing process are given in Appendix A of this report.

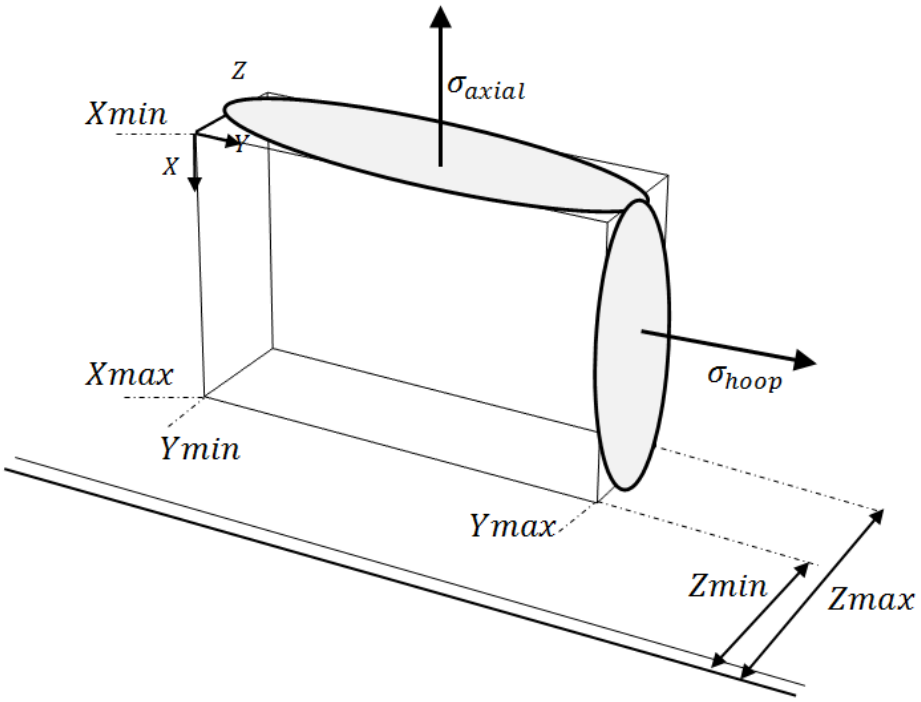

Fig. 5.7 Bounding box for flaw quasi-laminar indication showing the two resolved fully elliptical flaws normal to the axial and circumferential (hoop) principal stress directions.

5.6.3 Transient Loading – Pressure and Temperature

ORNL SIA analyses use the same pressure-temperature transients and binning criteria (see Fig. 5.4) as described earlier in *Section 5.3.4*. Plots of the five transients used by ORNL are given in Appendix B.

5.6.4 ORNL Acceptance Criteria for Characterized Flaws

ORNL uses versions of acceptance criteria given as follows:

Criterion *I* *ASME Section XI (1992)* ref. [5] (same as EBL analyses)

$$K_I < \frac{K_{IR}}{SF}, \tag{5.3}$$

where

$K_{IR} = K_{Ia}; SF = \sqrt{10}$ for level A/B transients (cool-down and heat-up)

$K_{IR} = K_{Ic}; SF = \sqrt{2}$ for level C/D transients (LOCAs)

K_{IR} = crack growth resistance fracture toughness

K_{Ia} = fracture arrest toughness

K_{Ic} = plane strain fracture toughness

Criterion *II ASME Section XI (2004)* Ref. [6]

$$K_I < \frac{K_{Ic}}{SF} \tag{5.4}$$

where

$SF = \sqrt{10}$ for level A/B transients (cool-down, heat-up) and

$SF = \sqrt{2}$ for level C/D transients (LOCAs)

In the *ASME Section XI (2004)* code, the plane strain fracture toughness, K_{Ic}, replaces the fracture arrest toughness, K_{Ia}, for level A/B transients.

ORNL applied the acceptance criteria to the re-generated flaw characterization files (*Section* 5.6.2) using the FAVOR v12.1 code and the screened pressure-temperature design transients (*Section* 5.6.3). Objectives of those applications include determination of an RT_{NDT} margin, measured relative to the applicable fracture toughness curve, for each individual flaw or grouped flaw subjected to the screened transient loading conditions. The latter calculation is analogous to the methodology applied by EBL in ref. [1] (see *Section* 3.5.3 of [1], *Crack Driving Forces*, pp. 41-44).

The ORNL methodology is explained through an example application given in Fig. 5.8, which shows the applied K_I versus time for *Flaw Group GP0817* in the Doel 3 Lower Shell subjected to the postulated LOCA transient. The analysis is conducted for the axially-oriented component (see Fig. 5.7) of *Flaw Group GP0817*.

Fig. 5.8 also shows three K_{Ic} lower bound fracture toughness curves (see Criteria *I* and *II* above) corresponding to three distinct values of increasing RT_{NDT} for the crack tip of the elliptical flaw that is nearest the wetted inner surface. Applied K_I for that flaw tip reaches maximum value of 68.6 MPa$\sqrt{}$m at time t =14 min. Fig. 5.8 illustrates how the K_{Ic} curve moves downward for increasing $RT_{NDT,}$ until it becomes tangent with the applied K_I curve, the point of tangency occurring in this case for RT_{NDT} = 65.4 °C. Embrittlement data [22] provided by EBL indicates the "final" RT_{NDT} = 88.4 °C; the corresponding fracture toughness curve is shown. Thus, the *Flaw Group GP0817* becomes critical for cleavage initiation before reaching "final" conditions; consequently, it does not satisfy the acceptance Criteria *I* and *II*.

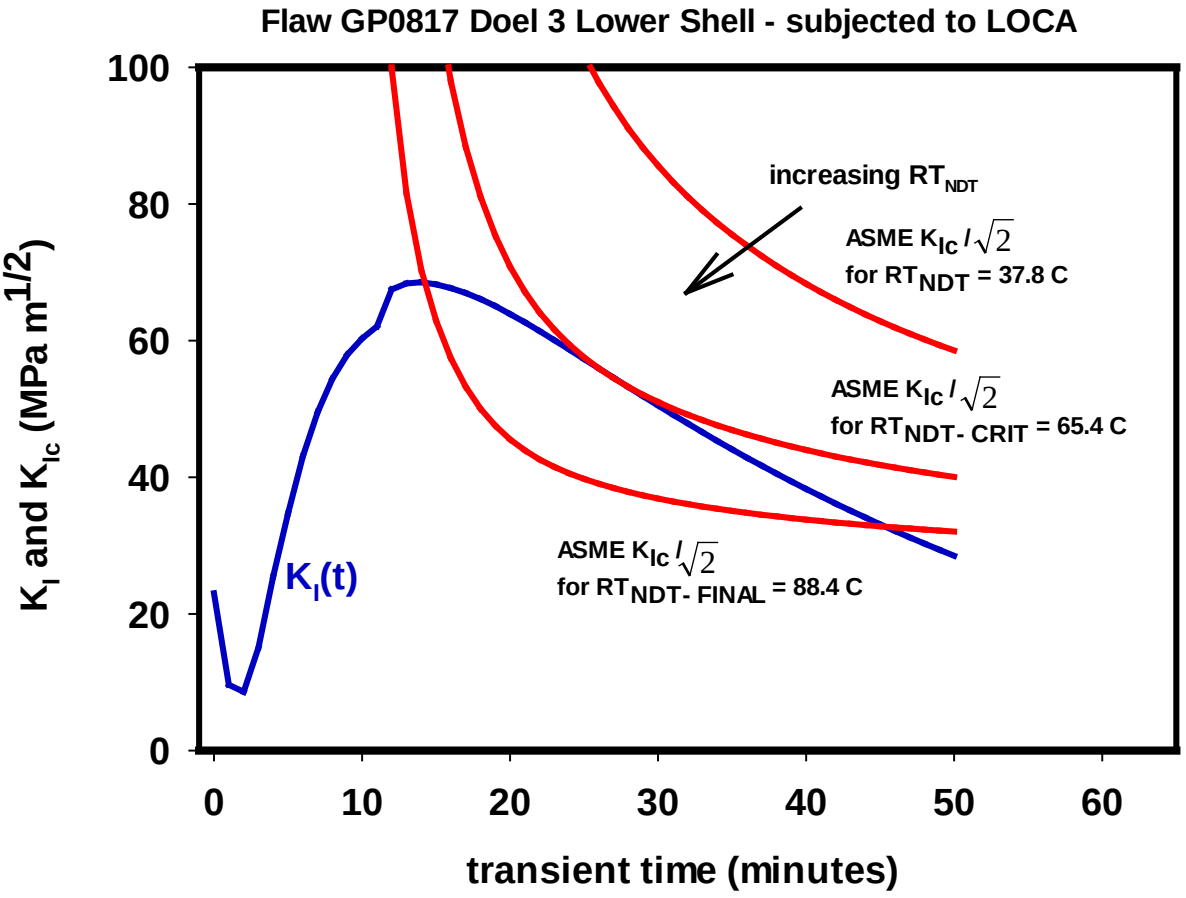

Fig. 5.8 Illustration of FAVOR solution methodology to determine the critical value of RT_{NDT} = 65.4 °C, i.e., the value of RT_{NDT} which creates a point of tangency between the ASME acceptance criterion $K_{IC}/\sqrt{2}$ curve and the applied K_I versus time curve.

Table 5.1 defines parameters used by ORNL in applications of the ASME Section XI acceptance criteria.

Table 5.1 Definition of parameters related to flaw acceptance criteria

Parameter	Definition
$\boldsymbol{RT_{NDT\text{-}CRIT}}$	critical value of $\boldsymbol{RT_{NDT}}$ that provides a point of tangency between the applied K_I and the applicable ASME lower bound fracture toughness curve
$\boldsymbol{RT_{NDT\text{-}FINAL}}$	"final" $\boldsymbol{RT_{NDT}}$ at "end-of-service-life"
$\boldsymbol{\Delta RT_{MARGIN}}$	$\boldsymbol{(RT_{NDT\text{-}CRIT} - RT_{NDT\text{-}FINAL})}$ margin term used for application of ASME flaw acceptance criterion • $\boldsymbol{\Delta RT_{MARGIN} > 0}$: acceptance criterion is satisfied • $\boldsymbol{\Delta RT_{MARGIN} < 0}$: acceptance criterion is not satisfied
$\boldsymbol{RT_{NDT\text{-}FINAL}/\ RT_{NDT\text{-}CRIT}}$	Alternative parameter for application of ASME flaw acceptance criterion • $\boldsymbol{RT_{NDT\text{-}FINAL}/\ RT_{NDT\text{-}CRIT} < 1}$: acceptance criterion is satisfied • $\boldsymbol{RT_{NDT\text{-}FINAL}/\ RT_{NDT\text{-}CRIT} > 1}$; acceptance criterion is not satisfied

For the example of *Flaw Group GP0817*, the parameters in Table 5.1 are determined to have the following values:

- $RT_{NDT\text{-}CRIT}$ = 65.4 °C,
- $RT_{NDT\text{-}FINAL}$ = 88.4 °C,
- ΔRT_{MARGIN} = - 23 °C, or
- $RT_{NDT\text{-}FINAL}/\ RT_{NDT\text{-}CRIT}$ = 1.35; thus, acceptance criterion is not satisfied.

5.6.5 ORNL Flaw Screening Results

Results of the ORNL flaw acceptance screening analysis performed for D3/T2 are reported in this section. Those ORNL analyses are based on the input data extracted from the body of EBL documentation as summarized in the foregoing sections. The ORNL analysis effort was focused on

a. performing an independent screening assessment of the entire population of flaws characterized by EBL, and
b. comparing the ORNL results with those from the EBL screening analysis.

For clarity, the sequence of steps employed in the ORNL screening assessment is briefly summarized below:

- All EBL-characterized flaws were re-generated according the methodology described in *Section* 5.6.2; thus, each EBL-characterized flaw was represented by two fully elliptical flaws normal to principal stress directions (axial and circumferential).

- The FAVOR code was used to analyze each of the fully elliptical flaws (both axial and circumferential) subjected to an EBL-specified primary system design transient; for a given flaw, that design transient was selected based on the ligament *S* (measured between the clad/base metal interface and the inner-most tip of the elliptical flaw) and the following binning criteria (see Fig. 5.4):

    - ligament *S* length 0 -20 mm – loss of coolant accidents (LOCAs), (black symbols in Figs. 5.9-5.14)
    - ligament *S* length 20-30 mm – cool-down transient, (blue symbols in Figs. 5.9-5.14)
    - ligament *S* length > 30 mm – heat-up transient. (red symbols in Figs. 5.9-5.14)

- Each elliptical flaw (axial and circumferential) was evaluated according to the ASME acceptance criteria *I* and *II* given in *Section* 5.6.4 using the FAVOR analysis results for the applicable design transient; that evaluation is based on determination of the ratio $RT_{NDT\text{-}FINAL}/\ RT_{NDT\text{-}CRIT}$ (see Table 5.1) for the flaw/transient combination.
- If either one of the fully elliptical flaws (axial or circumferential) fails to satisfy the acceptance criterion, then the corresponding EBL-characterized flaw is designated as not satisfying that criterion

Results from application of ASME (1992) Criterion *I* (see *Section* 5.6.4) in the ORNL screening assessment are depicted as follows: Fig. 5.9- Doel 3 lower shell; Fig. 5.10- Doel 3 upper shell; and Fig. 5.11- Tihange 2. Analogous results from application of ASME (2004) Criterion *II* are shown in Fig. 5.12, Fig. 5.13 and Fig. 5.14, respectively. Each data point represents an EBL-characterized flaw, either a single or grouped (boxed) flaw.

Features of those plots include the following:

- Data point coordinates for each flaw are ($RT_{NDT\text{-}FINAL}/\ RT_{NDT\text{-}CRIT}$) versus (ligament length *S*).
- $RT_{NDT\text{-}CRIT}$ used in determining flaw acceptance is the lower of the two values computed by FAVOR for the axially and circumferentially oriented, fully elliptical components of the EBL-characterized flaw.
- Data points with ratio $RT_{NDT\text{-}FINAL}/\ RT_{NDT\text{-}CRIT} > 1$ do not satisfy the acceptance Criteria *I* or *II* given in *Section* 5.6.4.
- Very few of the EBL-characterized flaws were found to not satisfy the ASME (1992) acceptance criterion; even fewer flaws failed the ASME (2004) criterion.
- It should be noted that the data points in Fig. 5.9-5.14 include only those flaws for which $RT_{NDT\text{-}CRIT}$ exists. In order for $RT_{NDT\text{-}CRIT}$ to exist, the maximum value of $K_I(t)$ must be equal to or greater than the minimum (lower shelf) value of the applicable fracture toughness curve. There were many flaws that did not satisfy that criterion.

Table 5.2 provides additional data regarding those EBL-characterized flaws shown in Fig. 5.9-Fig. 5.14 that do not satisfy ASME (1992 and 2004) acceptance criteria. Those flaw data are grouped as follows:

- Table 5.2 (a) – flaws shown in Fig. 5.9 through Fig. 5.11 that are non-compliant based on ASME Sect. XI (1992 - Criterion *I*), and
- Table 5.2(b) – flaws shown in Fig. 5.12 through Fig. 5.14 that are non-compliant based on ASME Sect. XI (2004 - Criterion *II*).

In Table 5.2 (a), application of ASME (1992 – Criterion *I*) produced 17 non-compliant flaws for the two plants, where

- most non-compliant flaws are located in the Doel 3 lower shell and are due to cool-down and heat-up transients (five due to cool-down and eight due to heat-up), and
- four flaws are non-compliant due to LOCAs (three in Doel 3 and one in Tihange 2).

In Table 5.2 (b), the less restrictive acceptance criterion for level A/B loading defined in ASME (2004 – Criterion *II*) resulted in all flaws being acceptable for cool-down and heat-up transients; results for LOCAs were the same as for ASME (1992 – Criterion *I*), as the acceptance criterion is unchanged.

Effects of Invoking Warm-Prestress (WPS) in ORNL Screening Assessments: In Appendix C, the WPS model implemented into FAVOR [Ref. (20)] is invoked to re-assess the four EBL-characterized flaws listed in Table 5.2 (b) that are non-compliant according to ASME Section XI (2004). The three non-compliant EBL-characterized flaws found in Doel 3, i.e., Flaw Groups GP0817 and GP0818, as well as individual flaw 492, are shown to be compliant with application of the WPS model. For the individual flaw 1660, found in Tihange 2 and subjected to LOCA 1, the screening criterion $RT_{NDT\text{-}FINAL}/RT_{NDT\text{-}CRIT}$ decreases from 1.49 to 1.20; thus, flaw 1660 remains non-compliant according to the ASME acceptance criterion with or without WPS.

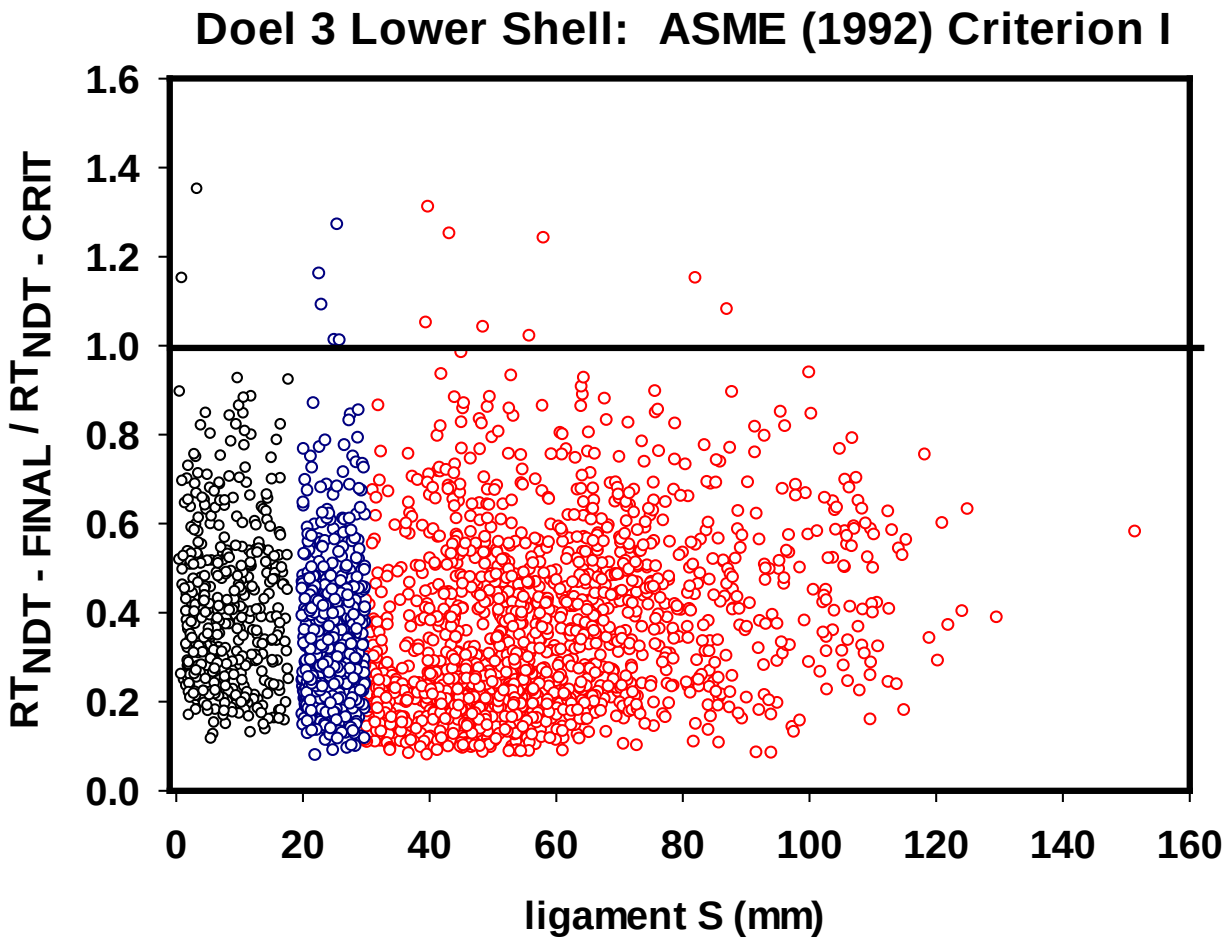

Fig. 5.9 ASME(1992) Criterion *I*: ORNL Flaw Acceptance Analysis – Doel 3 Lower Shell (see Section 5.6.5 for details regarding this figure).

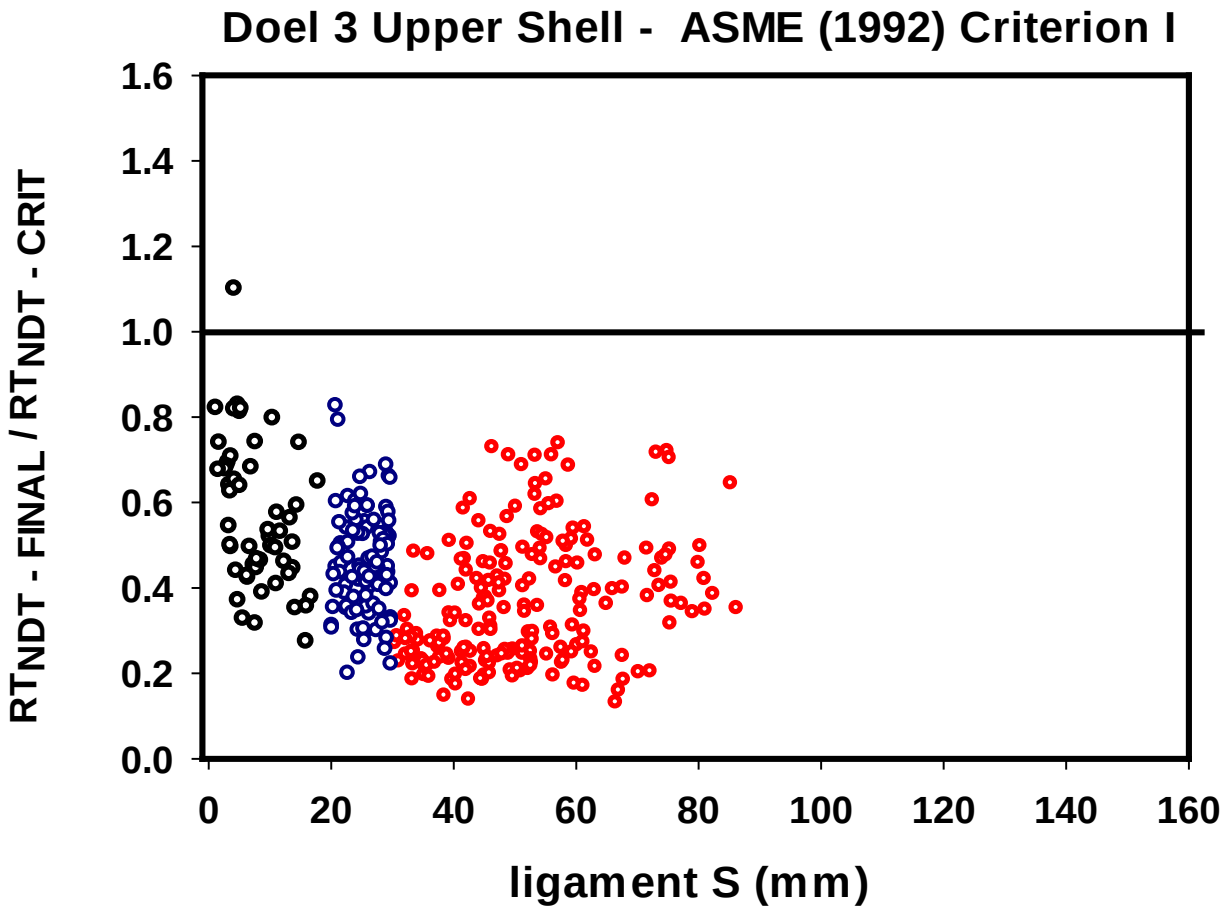

Fig. 5.10 ASME (1992) Criterion *I*: ORNL Flaw Acceptance Analysis – Doel 3 Upper Shell (see Section 5.6.5 for details regarding this figure).

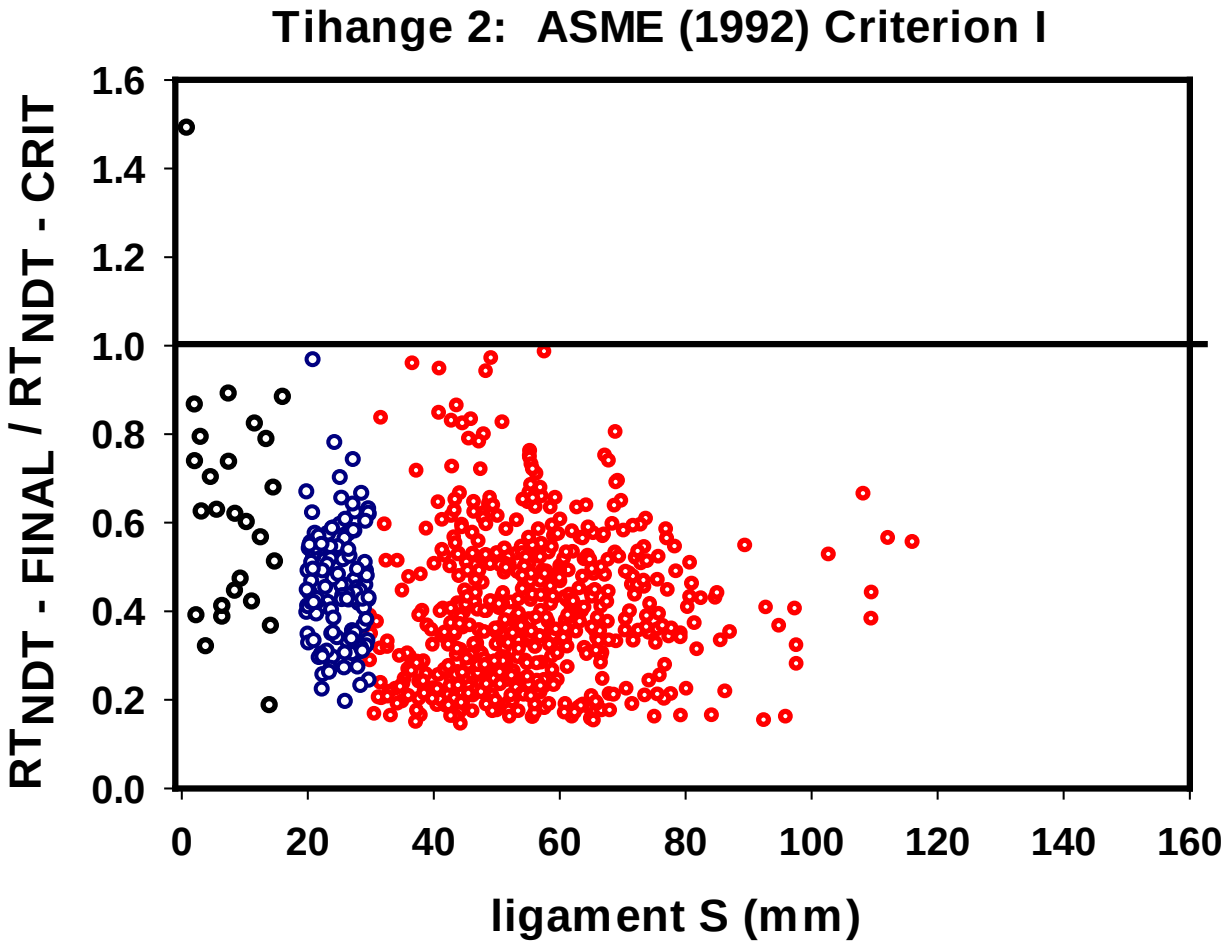

Fig. 5.11 ASME (1992) Criterion *I*: ORNL Flaw Acceptance Analysis – Tihange 2 (see Section 5.6.5 for details regarding this figure).

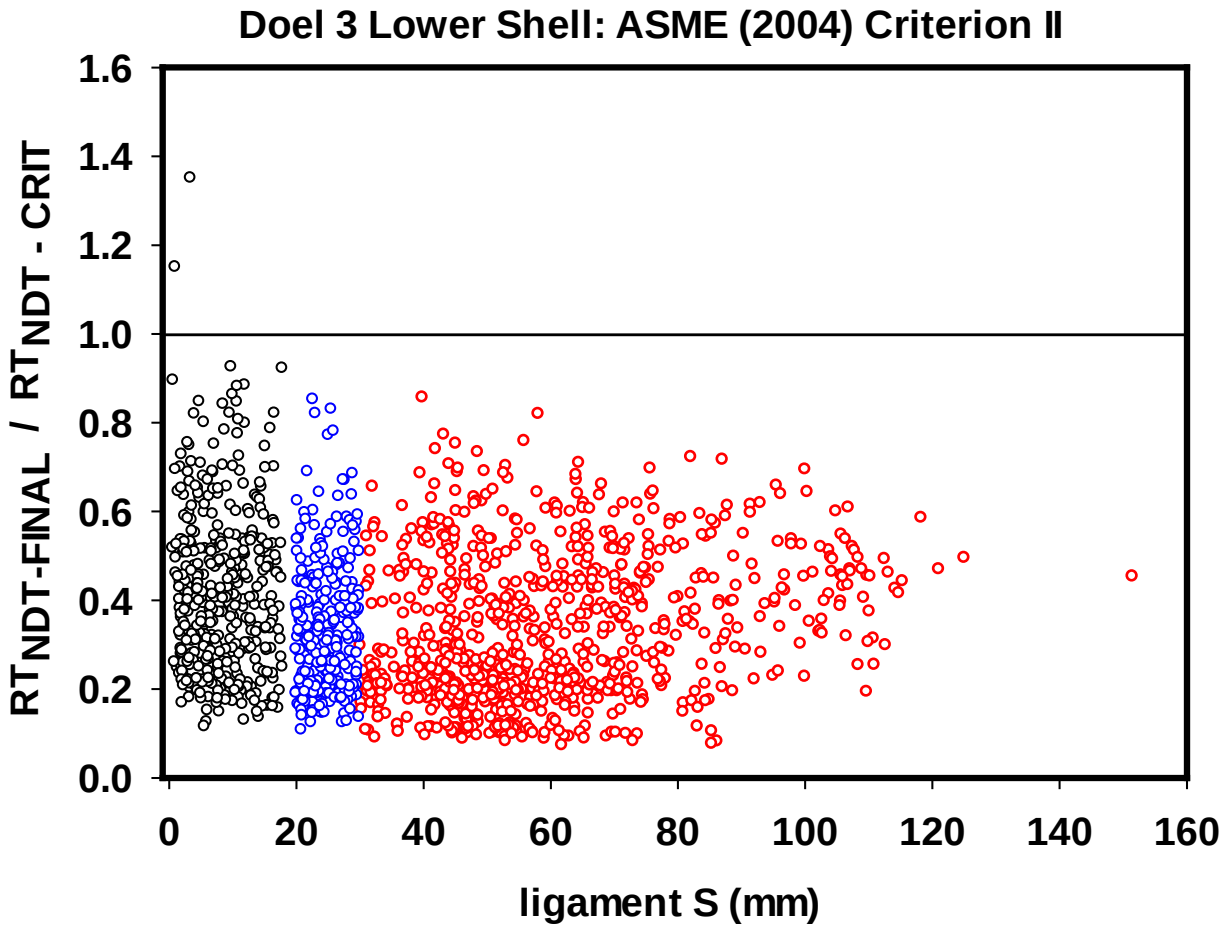

Fig. 5.12 ASME (2004) Criterion *II*: ORNL Flaw Acceptance Analysis – Doel 3 Lower Shell (see Section 5.6.5 for details regarding this figure).

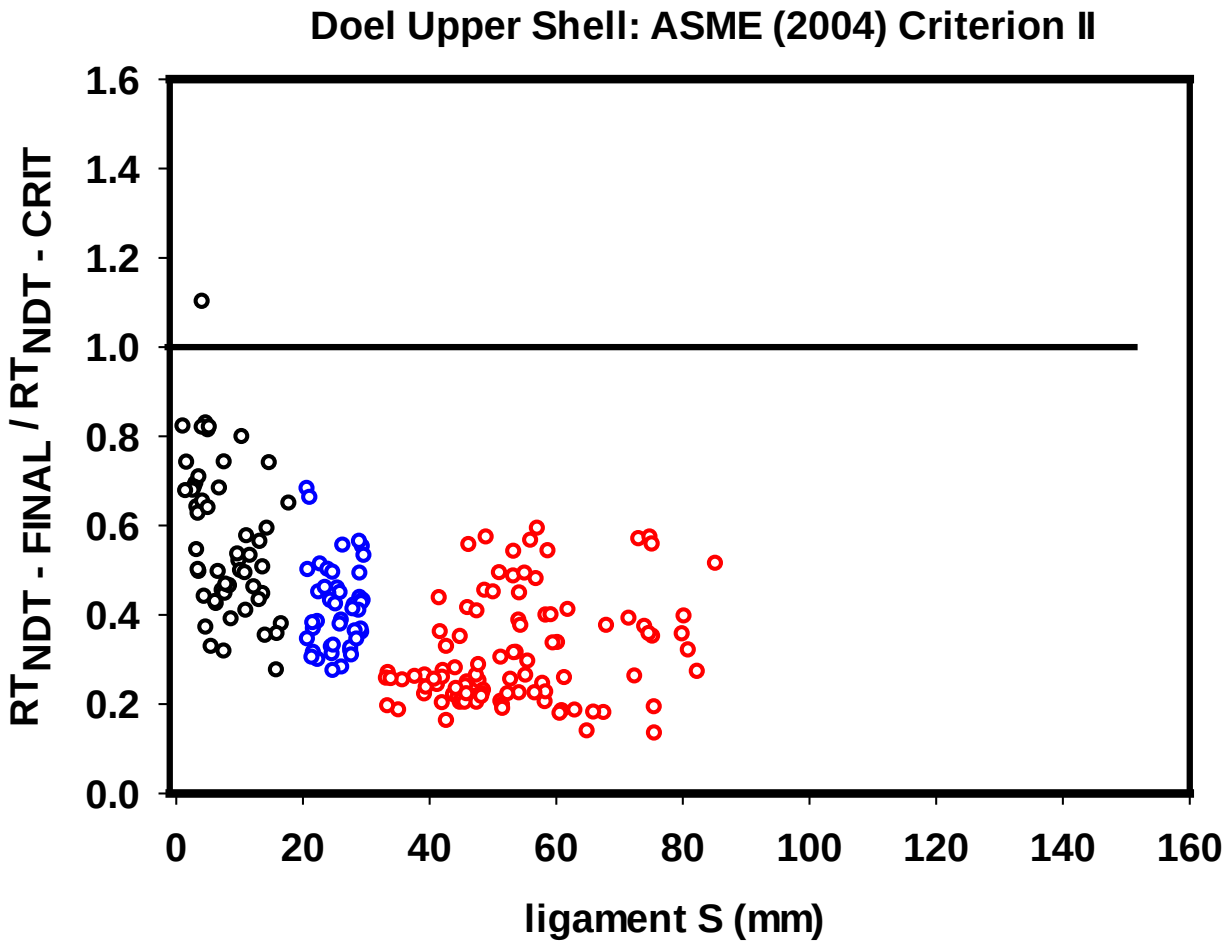

Fig. 5.13 ASME (2004) Criterion *II*: ORNL Flaw Acceptance Analysis – Doel 3 Upper Shell (see Section 5.6.5 for details regarding this figure).

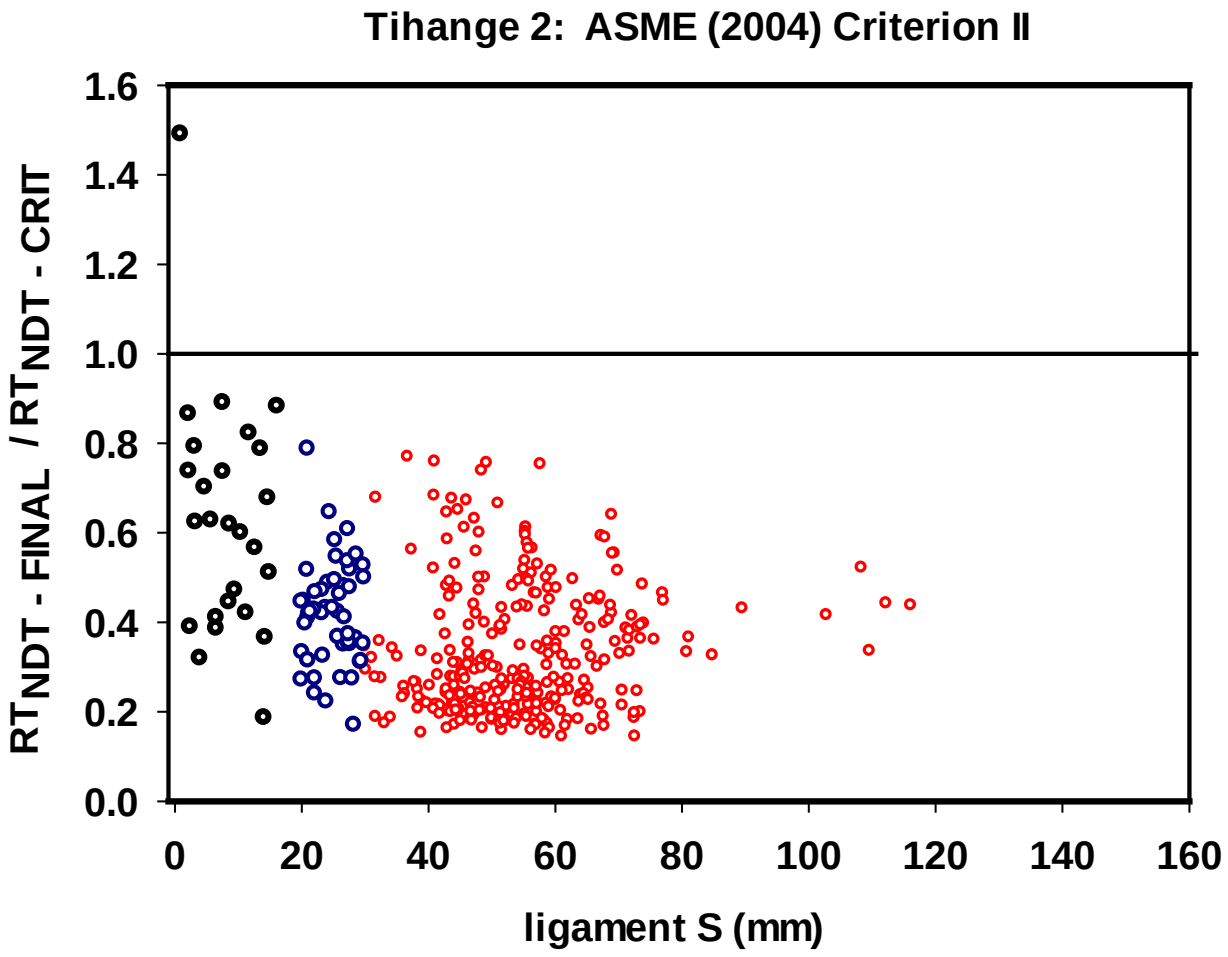

Fig. 5.14 ASME (2004) Criterion *II*: ORNL Flaw Acceptance Analysis – Tihange 2 (see Section 5.6.5 for details regarding this figure).

Table 5.2 ORNL screening summary of EBL characterized flaws not satisfying ASME acceptance criteria

Table 5.2(a) ASME Section XI (1992) – Criterion *I*

(Highlighted flaws were determined to be non-compliant in the EBL screening assessment)

Doel 3 Lower Shell

Plant	Region	Transient	ASME Criterion	FLAW ID	Flaw ligament (mm)	$RT_{NDT-FINAL}$ (°C)	$RT_{NDT-CRIT}$ (°C)	Ratio $RT_{NDT-FINAL}$ / $RT_{NDT-CRIT}$
Doel	Lower	CD	I	GP0474	25.53	63.57	50.18	1.27
Doel	Lower	CD	I	GP0792	22.69	87.32	75.39	1.16
Doel	Lower	CD	I	GP0773	25.11	79.86	78.81	1.01
Doel	Lower	CD	I	GP0794	23.07	87.17	80.23	1.09
Doel	Lower	CD	I	GP0164	25.94	86.01	85.48	1.01
Doel	Lower	HU	I	GP0689	43.24	58.92	47.18	1.25
Doel	Lower	HU	I	GP0539	39.56	51.34	48.86	1.05
Doel	Lower	HU	I	GP0929	39.86	74.66	57.11	1.31
Doel	Lower	HU	I	GP0645	82.10	50.80	44.33	1.15
Doel	Lower	HU	I	GP0936	58.13	68.79	55.46	1.24
Doel	Lower	HU	I	GP0389	48.58	63.72	61.16	1.04
Doel	Lower	HU	I	GP0673	87.11	53.51	49.52	1.08
Doel	Lower	HU	I	GP0949	55.89	74.94	73.55	1.02
Doel	Lower	LOCA	I	GP0817	3.41	88.32	65.44	1.35
Doel	Lower	LOCA	I	GP0818	1.00	89.32	77.92	1.15

Doel 3 Upper Shell

Plant	Region	Transient	ASME Criterion	FLAW ID	Flaw ligament (mm)	$RT_{NDT-FINAL}$ (°C)	$RT_{NDT-CRIT}$ (°C)	Ratio $RT_{NDT-FINAL}$ / $RT_{NDT-CRIT}$
Doel	Upper	CD	I	No transgressors				
Doel	Upper	HU	I	No transgressors				
Doel	Upper	LOCA	I	492	4.23	116.93	106.39	1.10

Tihange 2

Plant	Region	Transient	ASME Criterion	FLAW ID	Flaw ligament (mm)	$RT_{NDT-FINAL}$ (°C)	$RT_{NDT-CRIT}$ (°C)	Ratio $RT_{NDT-FINAL}$ / $RT_{NDT-CRIT}$
Tihange	-	CD	I	No transgressors				
Tihange	-	HU	I	No transgressors				
Tihange	-	LOCA	I	1660	0.95	110.98	74.28	1.49

Table 5.2 (b) ASME Section XI (2004) – Criterion *II*

Doel 3 Lower Shell

Plant	Region	Transient	ASME Criterion	FLAW ID	Flaw ligament (mm)	$RT_{NDT-FINAL}$ (°C)	$RT_{NDT-CRIT}$ (°C)	Ratio $RT_{NDT-FINAL} / RT_{NDT-CRIT}$
Doel	Lower	CD	II	No transgressors				
Doel	Lower	HU	II	No transgressors				
Doel	Lower	LOCA	II	GP0817	3.41	88.32	65.44	1.35
Doel	Lower	LOCA	II	GP0818	1.00	89.32	77.92	1.15

Doel 3 Upper Shell

Plant	Region	Transient	ASME Criterion	FLAW ID	Flaw Ligament (mm)	$RT_{NDT-FINAL}$ (°C)	$RT_{NDT-CRIT}$ (°C)	Ratio $RT_{NDT-FINAL} / RT_{NDT-CRIT}$
Doel	Upper	CD	II	No transgressors				
Doel	Upper	HU	II	No transgressors				
Doel	Upper	LOCA	II	492	4.23	116.93	106.39	1.10

Tihange 2

Plant	Region	Transient	ASME Criterion	FLAW ID	Flaw ligament (mm)	$RT_{NDT-FINAL}$ (°C)	$RT_{NDT-CRIT}$ (°C)	Ratio $RT_{NDT-FINAL} / RT_{NDT-CRIT}$
Tihange	-	CD	II	No transgressors				
Tihange	-	HU	II	No transgressors				
Tihange	-	LOCA	II	1660	0.95	110.98	74.28	1.49

5.6.6 Comparison of ORNL and EBL Screening Analysis Results

Results from ORNL screening assessments of D3/T2, given in Fig. 5.9-Fig. 5.14 and Table 5.2, are compared herein to the EBL assessments. Histograms of the EBL screening results are shown in Fig. 5.5, indicating a total of 28 non-compliant characterized flaws for Doel 3 and nine for Tihange 2; the EBL screening assessments are based solely on ASME Section XI (1992 – Criterion *I*). Table 5.3 compares the total number of EBL-characterized flaws found not compliant with ASME acceptance criteria in the EBL and ORNL analyses; totals are broken down for each plant and, in the case of ORNL analyses, according to ASME 1992 and 2004 acceptance criteria.

Details concerning the non-compliant flaws identified in the EBL screening assessments are given in Table 5.4, Table 5.5, and Table 5.6, the latter tables taken from Refs. [22-23]. Some observations concerning the comparison of ORNL and EBL screening results include the following:[5]

- ORNL screening assessment is stated in terms of computed $RT_{NDT\text{-}CRIT}$ (see Table 5.2); EBL assessment is stated in terms of acceptable flaw size (see Table 5.4-Table 5.6).
- ORNL analysis results were similar to those of EBL in that few characterized flaws were found not compliant with the ASME (1992) acceptance criterion.
- ORNL screening analyses identified fewer non-compliant flaws than EBL (ORNL total number was 46 percent of EBL total for ASME Section XI (1992 – criterion *I*); ORNL application of ASME Section XI (2004 – criterion *II*) produced only four non-compliant flaws, all due to LOCAs.
- ORNL surmises that the greater number of non-compliant, characterized flaws identified in the EBL screening is due principally to the significantly more restrictive criterion for their assumed circular flaws, $2a < 0.5 \times 2a_{acc}$, employed by EBL for flaw size acceptance, described herein in *Section* 5.3.6; other possible contributors to this outcome in screening results are differences in the analysis methodologies used by ORNL and EBL.
- A total of 13 non-compliant flaws on the ORNL list (Table 5.2) are also found on the corresponding EBL summary (Table 5.4-Table 5.6); flaws common to both lists are highlighted in Table 5.2(a).

[5] Values of "Ligament *S*" quoted by ORNL (in Table 5.2) and by EBL (in Tables 5.4, 5.5, and 5.6) reflect slightly different distances from the clad/base metal interface to the inner crack tip. The ORNL values are slightly smaller because the ellipse used by ORNL to represent the flaw lies slightly outside the rectangle of the EBL boxed flaw along the major and minor axes, as seen in Fig. A.4 in Appendix A of this report. That difference in distance to the flaw tip is also reflected in a slightly different $RT_{NDT\text{-}FINAL}$ at the tip.

Table 5.3 Summary of number of EBL-characterized flaws that do not satisfy ASME acceptance criteria: EBL and ORNL screening analysis results

Organization	EBL	ORNL	
ASME Criteria	I (1992)	I (1992)	II (2004)
Doel 3	28	16	3
Tihange 2	9	1	1
Total	37	17	4

Table 5.4 EBL Non-Compliant Flaws: Doel 3 Lower Shell

(Table 2 in ref [22]. Lower Core Shell of Doel 3: Results of Structural Analysis)

Name	#Indic	Ligament (mm)	Angle (°)	Fluence (10^{19}n/cm²)	RT_{NDT} (°C)	Size 2a (mm)	$2a_{acc}$ (mm)	$2a/2a_{acc}$
GP0689	33	46.34	20.95	1.35	58.35	256.58	180.16	1.42
GP0078	5	50.94	35.24	1.11	53.55	132.70	103.74	1.28
GP0817	3	4.21	24.05	3.23	88.19	57.84	48.15	1.20
GP0645	9	84.10	21.87	0.97	50.60	189.25	168.81	1.12
GP0949	4	57.07	27.95	2.30	74.74	96.35	88.70	1.09
GP0827	3	55.42	29.38	1.39	59.23	107.38	108.16	0.99
GP0773	3	26.04	21.80	2.63	79.72	130.10	135.80	0.96
GP0134	7	33.47	18.94	1.82	66.88	177.89	195.85	0.91
GP0539	38	42.56	9.37	0.98	50.92	503.68	561.69	0.90
GP0936	9	60.02	16.20	1.91	68.42	194.09	220.70	0.88
GP0389	10	50.47	15.41	1.62	63.40	199.52	264.44	0.75
GP0929	19	42.32	11.02	2.25	74.03	231.09	309.10	0.75
GP0441	5	43.74	18.94	0.08	22.79	209.82	283.29	0.74
GP0474	23	27.93	10.24	1.60	63.12	276.89	393.28	0.70
GP0157	3	50.58	28.32	2.56	78.67	57.61	81.97	0.70
GP0771	4	54.12	19.08	2.02	70.23	114.30	165.03	0.69
GP0907	2	59.08	17.51	1.43	59.88	154.90	223.76	0.69
GP0789	3	50.47	17.28	2.45	77.01	115.04	179.58	0.64
GP0321	9	19.31	17.25	1.74	65.60	155.72	248.23	0.63
GP0280	2	43.98	12.66	2.60	79.32	151.40	253.82	0.60
GP0792	5	23.68	17.63	3.15	87.12	92.79	165.77	0.56
GP0407	9	49.52	8.00	1.47	60.74	218.96	392.94	0.56
GP0662	28	15.77	10.83	0.33	33.47	361.60	656.95	0.55
GP0920	7	33.95	14.01	1.19	55.21	203.37	383.50	0.53
GP0462	8	65.69	12.18	1.12	53.84	209.76	398.98	0.53
GP0795	4	46.22	19.04	3.10	86.47	67.76	130.71	0.52
GP0146	3	46.10	23.12	2.05	70.73	68.06	132.70	0.51

Table 5.5 EBL Non-Compliant Flaws: Doel 3 Upper Shell

(Table 1 in ref. [22] Upper Core Shell of Doel 3: Results of Structural Analysis)

Name	#Indic	Ligament (mm)	Angle (°)	Fluence (10^{19}n/cm²)	RT_{NDT} (°C)	Size 2a (mm)	$2a_{acc}$ (mm)	$2a/2a_{acc}$
Ev492	1	4.45	10.61	5.47	116.80	48.33	89.33	0.54

Table 5.6 EBL Non-Compliant Flaws – Tihange 2 Upper Shell

(Table 1 in ref. [23] Upper Core Shell of Tihange 2: Results of Structural Analysis)

Name	#Indic	Ligament (mm)	Angle (°)	Fluence (10^{19}n/cm²)	RT_{NDT} (°C)	Size 2a (mm)	$2a_{acc}$ (mm)	$2a/2a_{acc}$
GP0091	12	41.73	3.33	3.96	95.84	211.62	242.99	0.87
GP0086	7	50.11	6.87	3.12	84.08	211.06	278.70	0.76
GP0089	8	34.65	3.57	4.38	101.43	153.15	228.07	0.67
GP0126	2	25.69	30.55	3.15	84.43	40.68	65.85	0.62
1660	1	1.14	20.00	5.14	110.87	8.94	14.78	0.60
GP0115	8	58.61	5.61	2.79	78.99	170.84	288.60	0.59
GP0125	5	44.68	15.22	2.52	74.77	122.98	228.65	0.54
GP0095	6	69.46	4.04	2.57	75.48	156.60	293.67	0.53
GP0111	3	49.29	13.93	3.15	84.44	112.79	214.57	0.53

5.6.7 ORNL Refined Analysis of Non-Compliant Flaw 1660

ORNL has performed a refined analysis of *Flaw 1660* (from Tihange 2) subjected to a LOCA loading transient; that flaw is listed in Table 5.2 as non-compliant with the ASME Section XI flaw acceptance criterion. Among all the flaws analyzed using FAVOR, the majority of those that did not meet the acceptance criteria were grouped flaws. There were only two individual flaws that failed the acceptance criteria – *Flaw 492* from Doel 3 upper shell, and *Flaw 1660* from Tihange 2. The latter was chosen for this analysis, since it had the highest $RT_{NDT\text{-}FINAL}$, and also the largest (negative) ΔRT_{MARGIN} among all the transgressors identified by the FAVOR calculations. In addition, this is the *only* flaw that remained non-compliant when analyzed using FAVOR by assuming warm-prestress. Details of this analysis are given in Appendix D. The ORNL analysis follows procedures analogous to those described in refs. [1, 22-25]:

- replace the large, tilted circular flaw shown in Fig. 5.2 with an ellipse fitting into the rectangular 3-D box;
- analyze that ellipse using 3-D finite element models based on ABAQUS/XFEM to calculate the applied K_I around the flaw as a function of time;
- determine whether the refined analysis of the more realistic tilted elliptical flaw satisfies the ASME Section XI flaw acceptance criterion 2004; and
- compare ORNL and EBL conclusions regarding code acceptance of *Flaw 1660* based on refined analyses reported by the respective organizations.

Figures 5.15 (a) and (b) present the results of an initial benchmarking exercise carried out by ORNL to determine if the XFEM methodology, as implemented in the ABAQUS commercial finite element code (v 6.14-1) ref. [26], could reproduce the applied K_I vs time histories calculated by the FAVOR, v12.1, code for the transient under study. In Figs. 5.15 (a) and (b), flaw 1660 is postulated to be a planar flaw in the axial and circumferential orientations, respectively. The good agreement shown in Figs. 5.15 (a) and (b) provided the necessary confidence to then pursue a refined XFEM analysis of the observed quasi-laminar (Q-L) orientation for flaw 1660.

The results of the ORNL Q-L flaw analysis are summarized in Fig. 5.16 (see Appendix D in this report for full details). By comparing the Q-L flaw 1660 applied K_I history (calculated by the ORNL XFEM analysis) to the ASME K_{Ic} curve (with safety factor of $\sqrt{2}$), it is clear that, by this analysis for the Q-L orientation, flaw 1660 will not initiate in cleavage fracture.

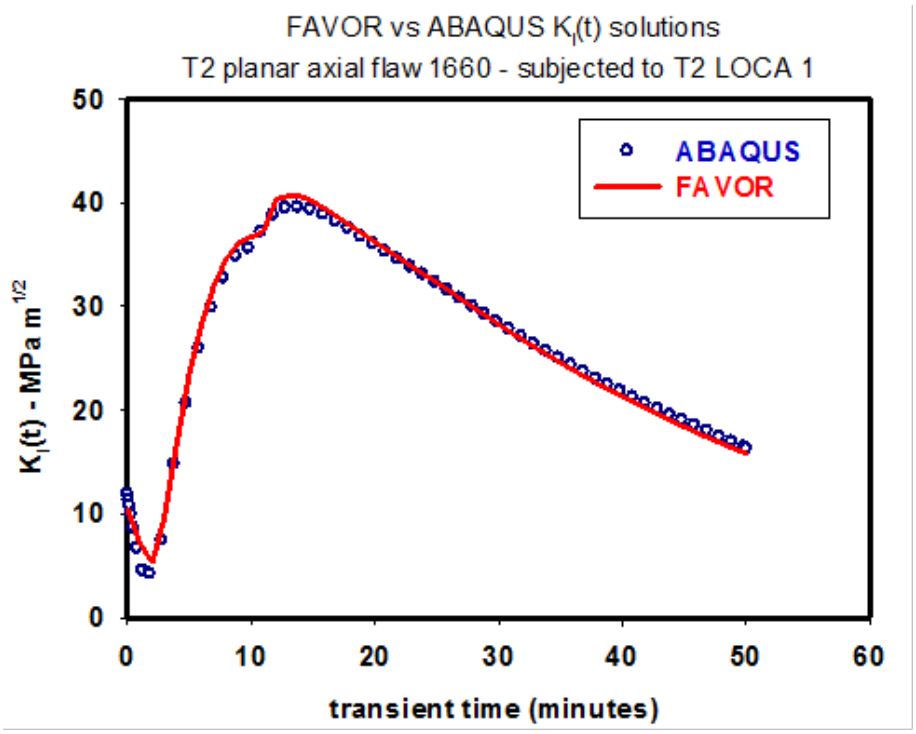

(a)

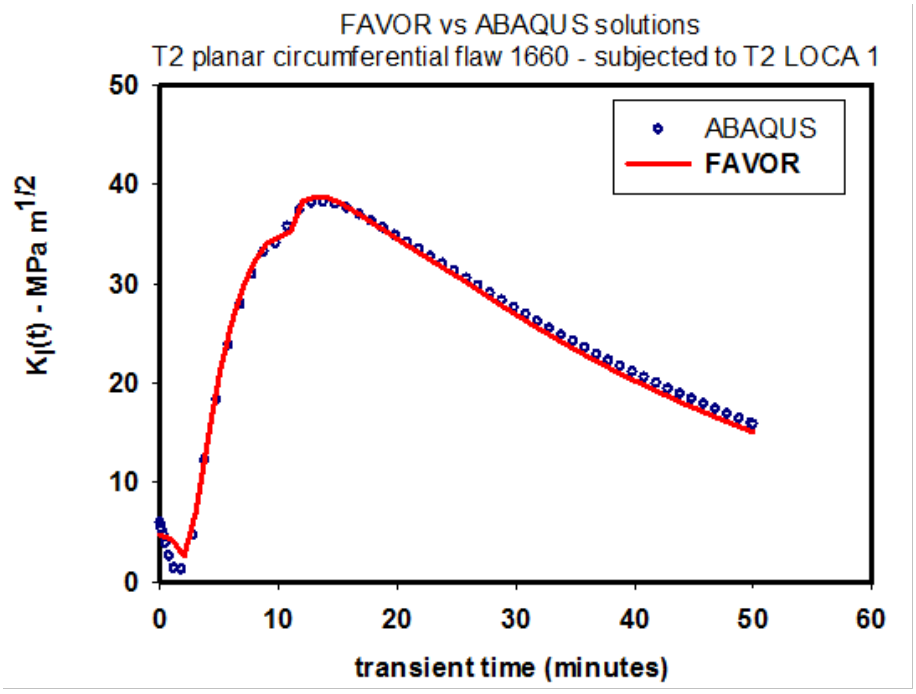

(b)

Fig. 5.15 Comparison of FAVOR with Abaqus XFEM $K_I(t)$ solutions for (a) axial and (b) circumferential embedded fully-elliptical planar flaws.

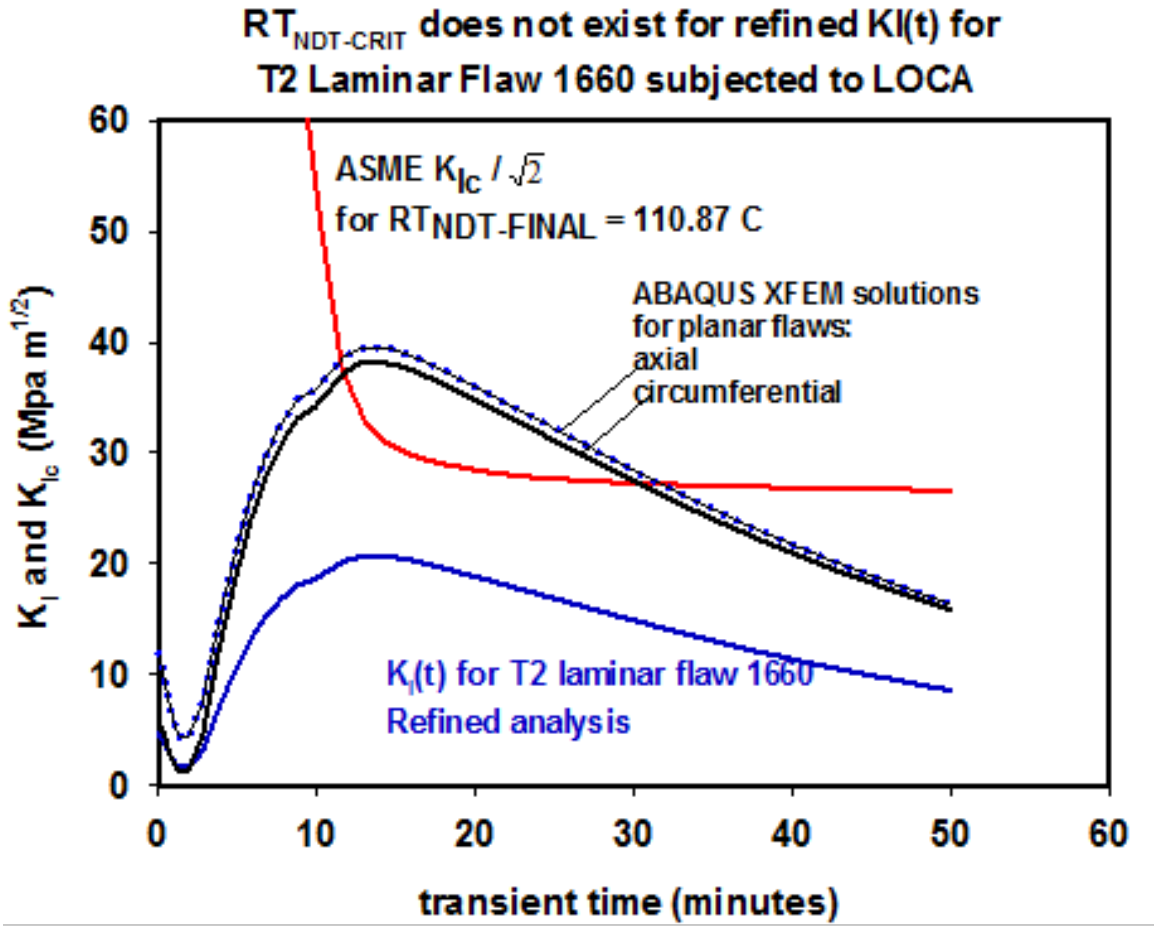

Fig. 5.16 Comparison of response of axial and circumferential planar flaws and quasi-laminar (Q-L) flaw 1660 to the applied transient. Overlay of the critical K_{Ic} curve indicates that the Q-L flaw is not predicted to initiate in cleavage fracture.

5.7 ORNL ASSESSMENT OF FATIGUE CRACK GROWTH ANALYSIS

EBL performed fatigue crack growth calculations in accordance with the ASME Code, Section XI, IWB-3610, following the general guidance given in the non-mandatory Appendix A, Analysis of Flaws, of Section XI [15-16]. The purpose was to establish the very limited, if any, potential for flaw growth by fatigue for the hydrogen flake defects. It is generally known that with the limited transients for a pressure vessel, even when a large flaw is evaluated, the amount of fatigue crack growth is small. The process that EBL followed was conservative in almost all steps of the calculations. Confirmatory calculations were not performed by ORNL as part of this evaluation, but based on the other confirmatory calculations performed by ORNL, the results reported by EBL are judged correct.

The following areas of major conservatism used by EBL are confirmed [15-16]:

- the use of circular flaws characterized in the 3-D boxes,
- the flaw categorization and determination of the reference flaws evaluated for fatigue crack growth,
- the axial projection method of the circular reference flaws to determine the stress intensity factors,
- the use of all design Level A and B transients covering the full 40 years,
- the assumed high value for the heat transfer coefficient, and
- not using a threshold ΔK for the calculations.

ORNL agrees with the EBL conclusion that the final larger amount of projected fatigue crack growth of 3.19% (Doel 3) is conservative and, in our estimation, very conservative.

5.8 ORNL ASSESSMENT OF ASME SECTION III PRIMARY STRESS RE-EVALUATION

It is important to confirm that the plastic collapse pressure (load) is greater than 1.5 times the design pressure for the vessel material that now has hydrogen flake defects embedded in the wall. The EBL evaluation is to confirm that the presence of the hydrogen flake defects does not invalidate the original ASME Code Section III design. EBL followed an acceptable method to verify the primary stress limits of Section III, NB-3000 with the inclusion of the hydrogen flakes defects reducing the local pressure membrane capacity of the material [17-18]. The EBL 2-D finite element calculations (plane strain) show a small reduction in the plastic collapse load of 26.9 MPa with no defects to 26.1 MPa for the highest density cell configuration with the largest sum of Z-axis projection dimensions (repeated 120 times at 3^{o} intervals). The minimum plastic collapse load for 1.5 times design pressure is 25.7 MPa. ORNL has not performed any verification calculations, but the process and illustrated results look reasonable and conservative. Therefore, ORNL is in agreement with the EBL calculations.

6. RESULTS OF TECHNICAL REVIEW OF SAFETY CASE

This section provides ORNL responses to FANC objectives for this report as stated in the work scope of Subtasks 1-6, presented herein in *Section* 2.1 - Subtasks. (It is noted here that the substantial analytical response generated by ORNL for the work scope outlined in Subtask 7 is addressed in its entirety in *Section* 5.)

1. *FANC: Assess the acceptability of each assumption considered by the licensee in the safety case except for the qualification of the ultrasonic instrument and the non-destructive examinations.*
   ORNL: Assumptions employed by the licensee that are considered by ORNL for comment include the following:

   - EBL flaw acceptance criterion was one-half of the ASME Section XI (1992) criterion, a very conservative assumption that resulted in a total of 37 non-compliant flaws. ORNL applied the ASME Section XI (1992 and 2004) criterion without any modification and identified only four flaws that did not satisfy ASME Section XI (2004). ORNL agrees with the EBL application of the ASME criterion.
   - EBL binned the design transients and boxed flaw ligaments according to a scheme depicted herein in Fig. 5.4. As a check on that scheme, ORNL performed analyses in which the transient / flaw binning illustrated in Fig. 5.4 was removed, i.e., all flaws were subjected to all design transients. While the latter action did increase the number of flaws for which a value of $RT_{NDT\text{-}CRIT}$ exists, it did not increase the number of flaws that were non-compliant with respect to the ASME screening criteria.
   - EBL identifies a list of conservatisms that are built into the input data and into the different steps of the SIA. In some cases, those conservatisms are quantified and imply that additional margins exist in the SIA; ORNL agrees with the assumptions in *Section* 6.5 of *2015 Doel 3 Safety Case.*
   - EBL's representation of flaw size for screening assessments defines the circular flaw that completely envelops the largest ellipse that fits into each 3-D flaw box. The latter procedure is recognized as a very conservative representation of a characterized flaw. Using that population of characterized flaws, ORNL assessments identified only four non-compliant flaws with respect to ASME Section XI.
   - EBL assumes the embrittlement shifts for D3 and T2 to be the same as those measured in the VB395 material. While that assumption has not been substantiated, it is considered to be very conservative. (See discussion in final paragraph *Section* 4.6 of this report).

2. *FANC: Assess the safety margins and the level of conservatism for the successive steps of the approach submitted by the licensee.*
   ORNL:

   - EBL presents a quantification of safety margins for the detected flaw populations of D3/T2; see *Section* 3.5 of ref. [1].
   - EBL describes the levels of conservatism in the successive steps of the SIA for D3/T2; see *Section* 3.5.7 of ref. [1].
   - Based on comparative evaluations of ORNL and EBL calculations for the SIA and on consideration of other results, ORNL is in agreement with the EBL conclusions that the safety margins and levels of conservatism are adequate to confirm structural integrity with respect to the entire population of defects.

3. *FANC: Identify any non-standard aspects for a safety justification of a nuclear RPV.*
   ORNL:

- EBL engaged in a major effort to develop suitable methodology to confirm the structural integrity of D3/T2 in the presence of large, dense populations of hydrogen flakes. Thus, EBL developed a methodology to account for the interaction of closely-space flaws, i.e., proximity rules. For the EBL screening assessments, the flaws are characterized either as individual or as grouped flaws and are placed in 3-D rectangular boxes that completely contain the flaws. A single circular flaw is then defined for screening assessment that completely envelops the largest ellipse that fits in that box with an appropriate tilt based on the box dimensions.
- EBL binned the design transients and boxed flaw ligaments according to a scheme depicted herein in Fig. 5.4; flaws are then analyzed with cool-down, heat-up or LOCA design transients depending on ligament distance from the clad/base interface. However, ORNL analyses indicate that whether or not the flaws are binned has no influence on the outcome of the SIA.

4. *FANC: Identify the new techniques developed by the licensee.*
ORNL: Non-standard aspects of the EBL SIA effort to confirm the structural integrity of D3/T2 (described above in response to subtask 3) involved at least some development of new techniques. No additional elaboration is necessary here.

5. *FANC: Assess the acceptability of these non-standard aspects and new techniques in the successive steps of the justification of the structural integrity of the RPVs.*
ORNL: Much of the EBL methodology used to analyze the non-standard quasi-laminar flaw populations in D3/T2 is incorporated into the ASME Code Case N-848, "Alternative Characterization Rules for Quasi-Laminar Flaws". Thus, the EBL methodology for assessing quasi-laminar flaws is backed by the ASME Boiler & Pressure Vessel Code. That same methodology was the basis for ORNL's evaluation of the EBL SIA.

6. *FANC: Identify:*
(a) The mistakes.
ORNL: None identified
(b) The questionable and unjustified aspects.
ORNL: None identified
(c) The questionable and justifiable – though lightly justified and documented – aspects in the safety case.
ORNL: None identified

7. SUMMARY AND CONCLUSIONS

This report presents an ORNL evaluation of the EBL structural integrity assessment of D3/T2 RPVs. Chapter 2 provides a statement of the overall objective of the ORNL effort, which is to perform a critical review of the EBL safety cases for the D3/T2 RPVs by assessing the existing safety margins against potential cracking in the RPVs due to the presence of almost laminar flaws in the walls. Detailed specification issued by the FANC for that ORNL effort are given in Subtasks 1 through 7 of that chapter:

- Subtasks 1-6 direct ORNL to assess the adequacy of specific elements of the EBL safety cases for D3/T2 as they relate to the objectives stated by EBL for those safety cases; the questions raised in Subtasks 1-6 are addressed by ORNL in Chapter 6; summary and conclusions are given below.
- Subtask 7 directs ORNL to perform structural integrity calculations with the same input parameters used by EBL, the specific purpose being to compare and verify analyses presented in the EBL safety cases; results from ORNL calculations and comparisons of the latter with analogous EBL calculations are described in Chapter 5.

Chapter 4 addresses certain compelling issues related to material properties of the D3/T2 RPVs that are crucial to the outcome of the structural integrity assessments described in Chapter 5. Conclusions drawn from discussions of specific topics in Chapter 4 include the following:

- Tests performed on flaked material (VB395 and KS02 forgings) show that the presence of flakes has no substantial impact on the mechanical properties as very similar results were obtained for specimens with flakes, for specimens taken between flakes, and for specimens taken outside the flaked area.
- Overall, the differences between the Master Curve fracture toughness reference temperature, T_0, and the Charpy V-notch index temperature, T_{41J}, measured on all tested materials in the unirradiated condition are within the scatter band observed on various RPV steels.
- The surveillance data from D3 and T2 demonstrate very good correspondence between the measured T_{41J} shifts and the predictions by the French RSE-M code predictive equation.
- Regarding the VB395 forging, very disparate results point to an extremely inhomogeneous material leading to the observation that the primary benefit from the testing of this material is that the hydrogen flakes did not substantially affect the fracture toughness of the material.
- The VB395 and KS02 materials are only relevant to D3/T2 primarily with regard to the fact that they each contain a high density of hydrogen flakes that is valuable in assessing if the hydrogen flakes have significant effects on the mechanical properties and fracture toughness of the D3/T2 forgings as a consequence of exposure to irradiation. The fact that Electrabel has applied an additional margin based on the behavior of the irradiated VB395 material is considered an additional conservatism.
- The root cause for the abnormal and excessive embrittlement of the VB395 forging is not thoroughly known at this time. Although not necessary for application to D3/T2, ORNL suggests that further research be conducted to discern the exact mechanism(s) of the abnormal embrittlement to provide additional knowledge regarding behavior of forgings with hydrogen flakes.
- A concern expressed by the International Review Board regarding the margin applied to the unirradiated RT_{NDT} for the D3/T2 materials resulted in Electrabel using a new approach to the overall margin with recent calculations showing that the current method has other built-in margins that compensate for this area of concern. ORNL is in agreement with the appropriately conservative margin applied by Electrabel in the Safety Cases.

Chapter 5 focuses on the ORNL evaluation of the EBL SIA performed as part of the safety cases for D3/T2 RPVs. The EBL SIA used applicable rules of the ASME Boiler & Pressure Vessel Code to confirm the

- absence of crack initiation for all individual flaws with adequate safety margins,
- stability of the flaws through fatigue crack growth evaluation, and
- primary stress intensity acceptance criteria.

Also, EBL performed a detailed evaluation of the level of conservatism present in each subtask of the SIA.

While Chapter 5 addresses each of the foregoing tasks, primary emphasis is given to assessment of potential crack initiation and existing safety margins in D3/T2. A series of analysis results from both EBL and ORNL are presented that collectively verify the absence of crack initiation for the D3/T2 flaw populations. Details of those assessments are provided in topics that sequentially

- summarize the specific parts of the EBL SIA focused on a screening assessment of the flaw population in D3/T2 when subjected to primary design transients,
- describe ORNL procedures for performing independent screening analyses of the entire EBL-characterized flaw population using EBL-provided input data,
- present and discuss ORNL results obtained from
  - application of ASME Section XI (both 1992 and 2004) to the EBL-characterized flaw population to identify flaws non-compliant with ASME acceptance criteria,
  - refined analyses of an EBL-characterized flaw (1660) that is non-compliant according to ASME Section XI but is rendered compliant when analyzed as an individual flaw using a more realistic 3-D XFEM model,
- compare and assess ORNL and EBL results from flaw screening assessments of characterized flaws that do not satisfy ASME flaw acceptance criteria, and
- compare and assess ORNL and EBL results from refined analyses that can confirm stability of the entire flaw population in D3/T2 with respect to brittle fracture.

Specific findings of the ORNL evaluation of that part of the EBL SIA focusing on stability of the flaw population subjected to primary design transients include the following results and conclusions derived from screening assessments and refined analyses.

Screening assessments:

- EBL screening assessments found that few characterized flaws in D3/T2 were not compliant with ASME (1992) acceptance criterion.
- ORNL screening analyses identified fewer non-compliant flaws than EBL; furthermore, ORNL applications of the more recent ASME Section XI (2004) produced only four non-compliant flaws, all due to LOCAs; when a warm-prestress model is invoked, only one characterized flaw (#1660) remains non-compliant.
- The finding of a greater number of non-compliant flaws in the EBL screening assessment is due principally to a significantly more restrictive (i.e., more conservative) criterion for flaw size acceptance used by EBL.
- Conclusion: ORNL screening assessment results for D3/T2 (obtained using different a analysis methodology) are interpreted herein as confirming the more conservative EBL screening results.

Refined analyses:

- EBL showed that all characterized flaws not compliant in the screening assessment meet the acceptance criterion with ample margin when subjected to refined analyses using 3-D XFEM models.
- ORNL demonstrated that the EBL-characterized flaw #1660,[6] which is non-compliant in both the ORNL and EBL screening assessments, is rendered compliant when modeled as a more realistic individual flaw using 3-D XFEM.
- ORNL and EBL refined analysis results are in good agreement for the individual flaw #1660 close to the clad/base metal interface; ORNL is not persuaded that repeating that exercise for more than one non-compliant flaw is necessary to accept EBL conclusions derived from the aggregate of EBL refined analysis results.
- Conclusion: ORNL interprets the refined analysis results provided by EBL for all originally non-compliant flaws, combined with the limited refined analysis results generated by ORNL, as being sufficient to declare the detected D3/T2 flaw population in compliance with the ASME Section XI acceptance criterion.

Final comments in Chapter 5 address two additional sets of calculations included in the EBL SIA:

- EBL assessments of the stability of the quasi-laminar flaws with respect to fatigue crack growth through end-of-service-life predicted maximum flaw growth of 3.19% for Doel 3 and 1.66% for Tihange 2.
- EBL performed an ASME Section III primary stress re-evaluation that accounted for the existing flaw population in D3/T2 and verified that the calculated collapse pressure is more than 1.5 times the design pressure as required by code.

Although ORNL did not perform verification calculations for those two assessments, the process and illustrated results appear reasonable and conservative. Thus, ORNL is in agreement with the conclusions reported by EBL for the foregoing elements of the SIA.

ORNL general conclusions regarding the SIA conducted by EBL for D3/T2 – Based on comparative evaluations of ORNL and EBL SIA calculations summarized herein and on consideration of other results, ORNL is in agreement with the general conclusions reported in *Section 3.6 General Conclusions* of ref. [1]. Specifically,

- more than 99 percent of flaws in D3/T2 meet the defined screening criterion, rendering them benign with respect to initiation in the event of a design transient;
- refined analyses of flaws that were non-compliant in that screening assessment indicate that 11 of the 16196 detected flaws have $K_{MAX} > K_{IR,\ lower\ shelf} / SF$; for those 11 flaws, the calculated margin in $RT_{NDT} > 80$ °C;
- fatigue crack growth is not a concern in the flaw acceptability analyses;
- primary stress re-evaluation confirms that the collapse pressure is more than 1.5 times the design pressure in the presence of defects detected in D3/T2; and

[6] Note that flaw #1660 is the only flaw in the ORNL screening assessment that is non-compliant with respect to ASME Section XI after the FAVOR WPS model is invoked (see Appendix C). In the US regulatory environment, there is general acceptance of the reality of WPS effects on cleavage fracture in pressure vessel steels. Thus, in that environment, the ORNL refined analysis result for flaw #1660 signifies that all D3/T2 detected flaws are ASME Section XI compliant when WPS is invoked.

- sufficient conservatisms are built into the input data and into the different steps of the SIA; in some cases, those conservatisms are quantified and imply that additional margins exist in the SIA.

Taken as a whole, the foregoing results and conclusions confirm the structural integrity of Doel 3 and Tihange 2 under all design transients with ample margin in the presence of the 16196 detected flaws.

8. REFERENCES

1. Doel 3/Tihange 2 Technical Summary Note Reactor Pressure Vessel Assessment, Electrabel report, April 14, 2015.

2. Safety Case 2015 Reactor Pressure Vessel Assessment, Doel 3, v.0, Electrabel report, dd. 17/07/2015.

3. Safety Case 2015 Reactor Pressure Vessel Assessment, Tihange 2, v.0, Electrabel report, dd. 17/07/2015.

4. Answers to FANC requests regarding margin on initial RT_{NDT}, outlier behaviour of VB395, and End-of-Life RT_{NDT} values of foreign reactors. Tractebel Engineering report CNT-KCD/4NT/22404/000/01, dd. 07/08/2014.

5. *ASME Boiler and Pressure Vessel Code – Section XI Rules for Inservice Inspection of Nuclear Power Plant Components*, American Society of Mechanical Engineers (1992), Two Park Avenue, New York, New York, USA.

6. *ASME Boiler and Pressure Vessel Code, Section XI, Appendix G*, "Fracture Toughness Criteria for Protection Against Failure," American Society of Mechanical Engineers (2004), New York.

7. Data provided to ORNL. Electrabel Document. September 2015.

8. Proximity rules for quasi-laminar flaws based on 3-D calculations. Tractebel Engineering report CNT-KCD/4NT/20374/000/01, dd. 30/07/2014.

9. V. Lacroix, P. Dulieu and D. Couplet, "Alternative Characterization Rules for Quasi-Laminar Flaws," Proceedings of ASME 2014 Pressure Vessels and Piping Division Conference, July 20-24, 2014, Anaheim, CA.

10. V. Lacroix, P. Dulieu and A. S. Bogaert, "Alternative Characterization Rules for Quasi-Laminar Flaws Based on 3-D X-FEM Calculations," Proceedings of ASME 2015 Pressure Vessels and Piping Division Conference, July 19-23, 2015, Boston, MA.

11. 4.1.2 – Doel 3: Transients synthesis from the design transients manual. Tractebel Engineering Report CNT-KCD/4NT/001772/000/03, dd. 29/10/2012.

12. 4.1.5 – Applicability of Doel 3 transients for Tihange 2 safety case. Tractebel Engineering report CNT-KCD/4NT/0017988/000/01, dd. 29/10/2012.

13. 4.3.6 – Calculations: RPV Doel 3: Structural assessment of the indications in Doel 3 reactor pressure vessel. Tractebel Engineering report CNT-KCD/4NT/0017845/0000/03, dd. 03/12/2014.

14. 4.3.8 – Calculations: RPV Tihange 2: Structural assessment of the indications in Tihange 2 reactor pressure vessel. Tractebel Engineering Report CNT-KCD/4NT/0018106/000/02, dd. 05/12/2014.

15. 4.6.1 – Calculations: RPV Doel 3: Fatigue Crack Growth Analysis. Tractebel Engineering report CNT-KCD/4NT/0017847/000/05, dd. 28/10/2014.

16. 4.6.2 – Calculations: RPV Tihange 2: Fatigue Crack Growth Analysis. Tractebel Engineering report CNT-KCD/4NT/0017960/000/03, dd. 28/10/2014.

17. 4.2.4– Calculations: RPV Doel 3 - ASME III elastic-plastic analysis. Tractebel Engineering report CNT-KCD/4NT/0018637/000/02, dd. 04/09/2014.

18. 4.2.4– Calculations: RPV Tihange 2 - ASME III elastic-plastic analysis. Tractebel Engineering report CNT-KCD/4NT/0018639/000/02, dd. 10/09/2014.

19. "Alternative Characterization Rules for Quasi-Laminar Flaws," *ASME Boiler and Pressure Vessel Code*, Case N-848, Section XI, Division 1, April 30, 2015.

20. P.T. Williams, T.L. Dickson, and S. Yin, *Fracture Analysis of Vessels – Oak Ridge FAVOR, v12.1, Computer Code: Theory and Implementation of Algorithms, Methods, and Correlations*, ORNL/TM-2012/567, Oak Ridge National Laboratory, Oak Ridge, TN, November 2012.

21. American Society of Mechanical Engineers Boiler and Pressure Vessel Code, *Section XI, Rules for Inservice Inspection of Nuclear Power Plant Components, Appendix A, Analysis of Flaws*, Article A-3000, Method for K_I Determination, American Society of Mechanical Engineers, New York, 1998.

22. 4.4.2 – Calculations: RPV Doel 3: 3-D multi-flaws and refined analyses. Tractebel Engineering Report CNT-KCD/4NT/0018107/000/02, (2014).

23. 4.4.2 – Calculations: RPV Tihange 2: 3-D multi-flaws and refined analyses. Tractebel Engineering Report CNT-KCD/4NT/0021061/000/00, (2014).

24. Pierre Dulieu et al, "Benchmark for the calculation of quasi-laminar elliptical cracks interaction under bi-axial loading," PVP2015-45788, Proceedings of the ASME 2015 Pressure Vessels and Piping Conference, PVP2015 July 19-23, 2015, Boston, Massachusetts.

25. Do-Jun Shim et al, "Application of extended finite element method (XFEM) to stress intensity factor calculations," PVP2015-45032, Proceedings of the ASME 2015 Pressure Vessels and Piping Conference, PVP2015 July 19-23, 2015, Boston, Massachusetts.

26. ABAQUS Finite Element Software, Version 6.14-1 (Standard), Dassault Systems Simulia Corp., Providence, RI (2014).

.

APPENDIX A. INPUT FILES FOR FAVOR ANALYSIS

Appendix A provides a description of the procedure used to generate input files for the FAVOR deterministic analysis starting with the data files provided by Electrabel. Along with the data files, a document "Data provided to ORNL," ref. [A.1], describing the files and the organization of the data in them was provided by Electrabel to help with data interpretation. As described in that document, the individual flaw indications as measured using UT were grouped according to the principles of the revised proximity rules given by the ASME Code Case N-848 [A.2]. The results of the grouping process were provided in the following Excel files:

- *Doel3-Grouping_Lower_Shell.xlsm* for Doel 3 Lower Core Shell
- *Doel3-Grouping_Upper_Shell.xlsm* for Doel 3 Upper Core Shell
- *Tihange2-Grouping_Core_Shells.xlsm* for Tihange 2 Lower and Upper Core Shells

These files were used as the starting point for the input file generation. In these files, the second tab, which is labelled "*KCD3_H(S-)=H(S+)=0.34_S=0.73*" in the files for Doel 3 and "*CNT2_H(S-)=H(S+)=0.34_S=0.73*" in the file for Tihange 2, contains data for the flaw indications after the grouping process. The data contained in columns V through AH were copied to another Excel file, with separate files created for Doel 3 lower and upper core shells, and one file for the Tihange 2 core shells. The first column contains an identification number, which starts with "GP" for a grouped set of flaw indications, or the indication ID number for an individual flaw. The next six columns are related to the minimum and maximum values (in mm) for the *X*, *Y* and *Z* coordinates of the box that encloses that particular grouped or individual flaw indication. Figure A.1, reproduced from ref. [A.1] illustrates the box specification. Here *X* is along the axial direction, *Y* is along the circumferential direction in angular coordinates measured in degrees, and *Z* is along the radial direction.

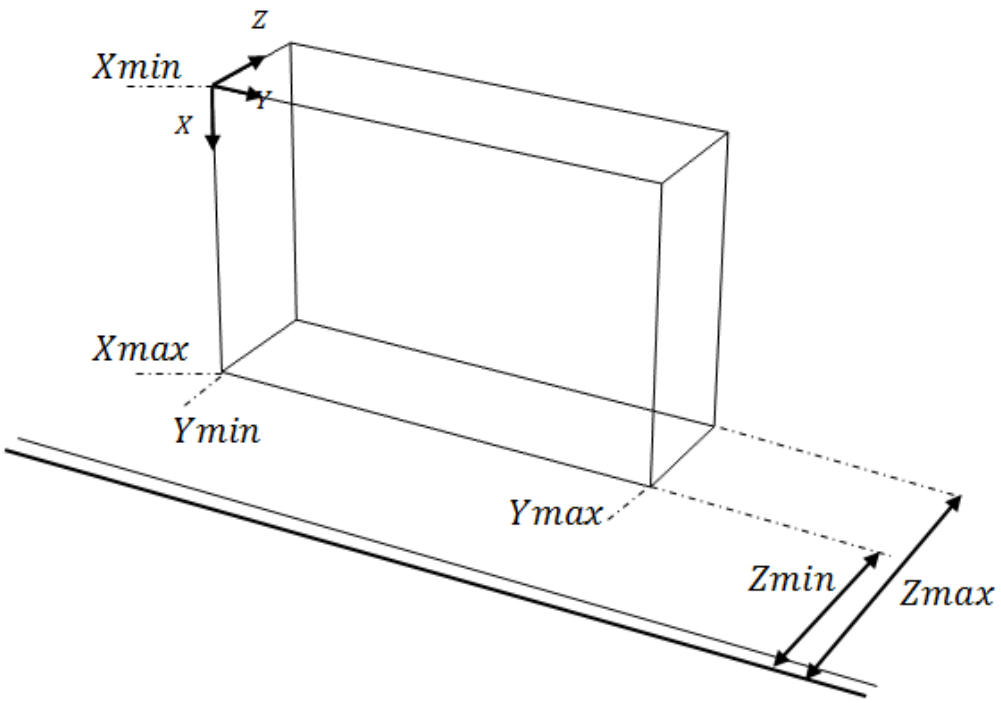

Fig. A.1 Coordinates used to specify the box bounding the flaw indication.

The next column (column H) contains the number of indications that are included in the group. Column I contains information that is not used. Columns J and K are the diagonals of the rectangular faces of the box parallel to the *XZ* (L_x) and *YZ* planes (L_y), respectively, as shown in Figure A.2. Columns L and M give the values of the angles made by the diagonals L_x and L_y with the XY plane (α_x, α_y), respectively. All data for columns A through M were taken from columns V through AH of the spreadsheet provided by Electrabel.

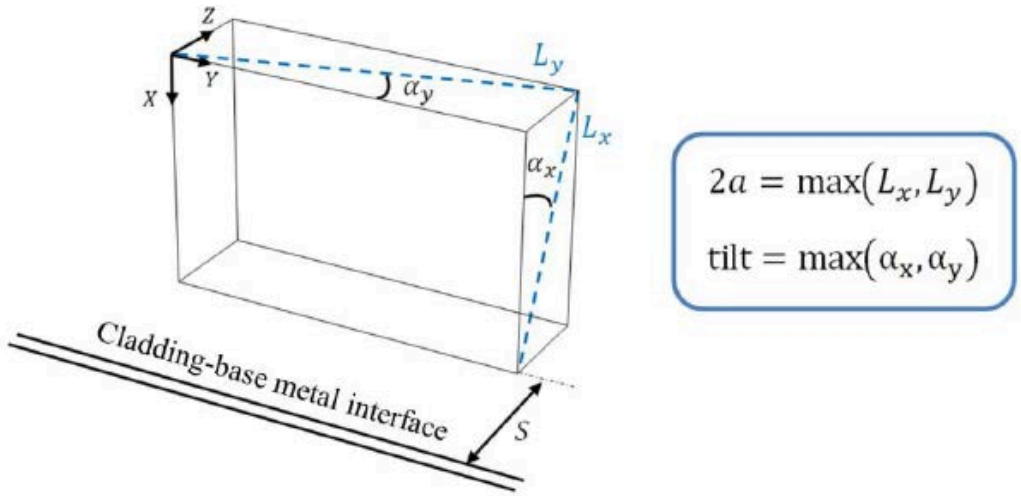

Fig. A.2 Diagonals and angles used to specify the flaw indication.

Based on the data for the bounding boxes containing the various flaw indications after the grouping procedure, the next step was to resolve the box into two elliptical planar flaws corresponding to the faces of the box normal to the principal stresses, which in this case are along the axial and circumferential directions. This approach is based on the ASME Code Case N-848, *Section* 5, which describes the resolved flaws as being rectangular in shape. However, the analysis using FAVOR requires flaws to be specified as elliptical, and therefore each of the rectangular planar flaws was replaced with an elliptical flaw, as indicated in Fig. A.3.

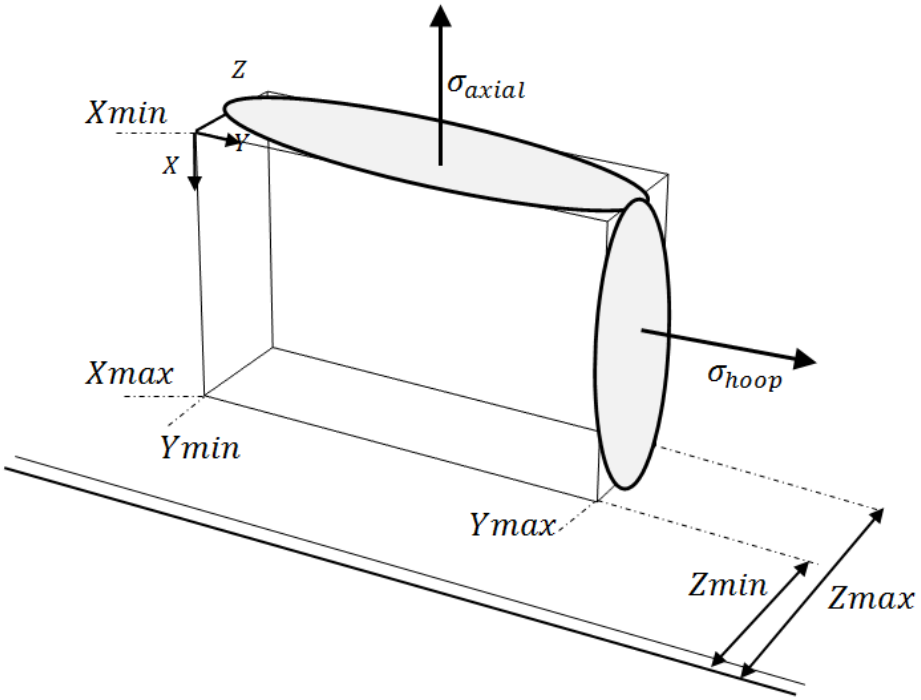

Fig. A.3 Bounding box for flaw indication showing the two resolved elliptical flaws normal to the axial and hoop stress directions.

In order to define the elliptical flaws, the criteria used was that the major axes of the ellipse are in the same ratio as the sides of the rectangle, and the area of the ellipse is the same as the area of the corresponding rectangle. Using these two criteria, it is possible to determine the major and minor axes of the ellipse. As shown in Fig. A.4, given a rectangle with sides *a* and *b*, we need to determine the semi-major and semi-minor axes *l* and *d*. The centers of the rectangle and ellipse are also assumed to be at the same point. If we require the major and minor axes of the ellipse to be in the same ratio as the length and width of the rectangle, and the area of the rectangle and ellipse to also be the same, then

$$\frac{a}{b} = \frac{l}{d} \text{ and } a \times b = \pi \times l \times d \ . \tag{5.5}$$

Using the above equations, we can find $l = a/\pi$ and $d = b/\pi$.

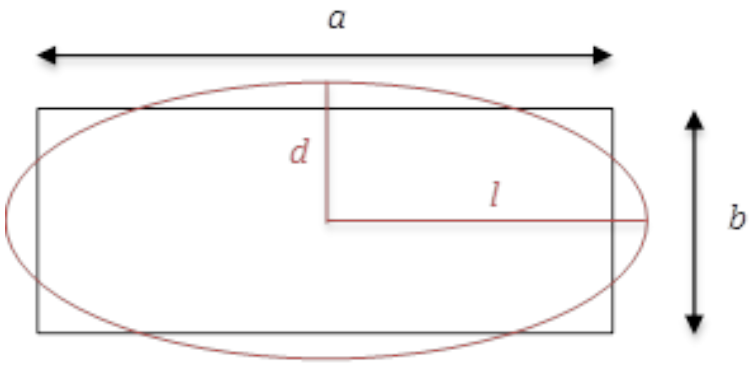

Fig. A.4 Rectangle and ellipse that have the same area and the same aspect ratio.

Columns N, O and P show the computed values of ΔX (=$X_{max} - X_{min}$), ΔY (=$Y_{max} - Y_{min}$) and ΔZ (= Z_{max} - Z_{min}), respectively. The value of ΔY was computed as the length of the circular arc at a radius halfway between Z_{max} and Z_{min}. Based on the dimensions of the rectangles, it was then possible to compute the relevant quantities for the elliptical flaws in the axial and circumferential directions. Columns Q and R show the computed values of L_x and L_y based on the values in columns N, O and P. These values were computed as a check to compare with the corresponding values in columns J and K that were copied from the data file provided by Electrabel.

The quantities needed by FAVOR to define the flaw geometry are the distance to the inner crack tip from the inside (pressure bearing) surface of the vessel, the depth and the aspect ratio of the flaw. Column S shows the distance to the inner crack tip (in inches), and the value differs slightly from Z_{min} because the ellipse lies slightly outside the rectangle along the major and minor axes, as seen in Figure A.4. Column T shows the flaw depth in inches. The values in columns S and T are the same for both the axial and circumferential flaws that are obtained from resolving each box. Columns U and V show the aspect ratios for the axial and circumferential flaws, respectively. Columns W and X show the final RT_{NDT} values in °F and °C, respectively. The values in column X were copied directly from column Z of the "Flaw_for_fluence" tab of the following files:

- *Doel3-Fluence_RTNDT.xlsx* for Doel 3 Core Shells
- *Tihange2-Fluence_RTNDT.xlsx* for Tihange 2 Core Shells

After some initial trial runs, it was determined that the RT_{NDT} values are needed at the inner crack tip, and therefore this value was computed based on the appropriate formula taken from the above files:

- Doel 3 upper core shell: RT_{NDT} = **-22 °C** + **39.5 $F^{0.59}$** + **31 °C**
- Doel 3 lower core shell: RT_{NDT} = **-22.2 °C** + **37 $F^{0.59}$** + **36.2 °C**
- Tihange 2 upper core shell: RT_{NDT} = **-25.4 °C** + **40 $F^{0.59}$** + **31 °C**
- Tihange 2 lower core shell: RT_{NDT} = **-27.2 °C** + **37.2 $F^{0.59}$** + **36.2 °C**

The fluence values shown in column Y were copied from column S of the "Fluence_for_fluence" tab for the corresponding files listed above. Following the procedure used in these files, the fluence value at the inner crack tip was computed by accounting for attenuation into the wall thickness (column Z), and the value was then extrapolated to end-of-service- life condition using the factor 1.21 (column AA). Column AB shows the computed RT_{NDT} based on the fluence value (second term in expression above). The final

RT_{NDT} at the inner crack tip is then computed from the fluence based value by adding the initial RT_{NDT} and a margin for uncertainty, and is listed in column AC after converting to °F.

A sorted version of the file was generated after sorting the flaws in order of decreasing flaw depth. The quantities needed for the FAVOR input file are columns S, T, U, V and AC. These columns have been copied into another tab (sheet 2), along with the first column for identifying the flaws. The data in these columns were then used to generate flaw list input file for FAVOR.

The other information needed for the FAVOR analysis is given in the data files related to the material properties and various loading transients. This information was obtained from the corresponding data files provided by Electrabel, and the data were modified to make the units consistent with units used in FAVOR.

APPENDIX A.1 REFERENCES

A.1 Data provided to ORNL. Electrabel Document. September 2015.

A.2 "Alternative Characterization Rules for Quasi-Laminar Flaws," *ASME Boiler and Pressure Vessel Code*, Case N-848, Section XI, Division 1, April 30, 2015.

APPENDIX B. PRIMARY SYSTEM TRANSIENTS

Appendix B presents the primary system transients provided by EBL for the screening assessment of D3/T2 RPVs (Ref. B.1).

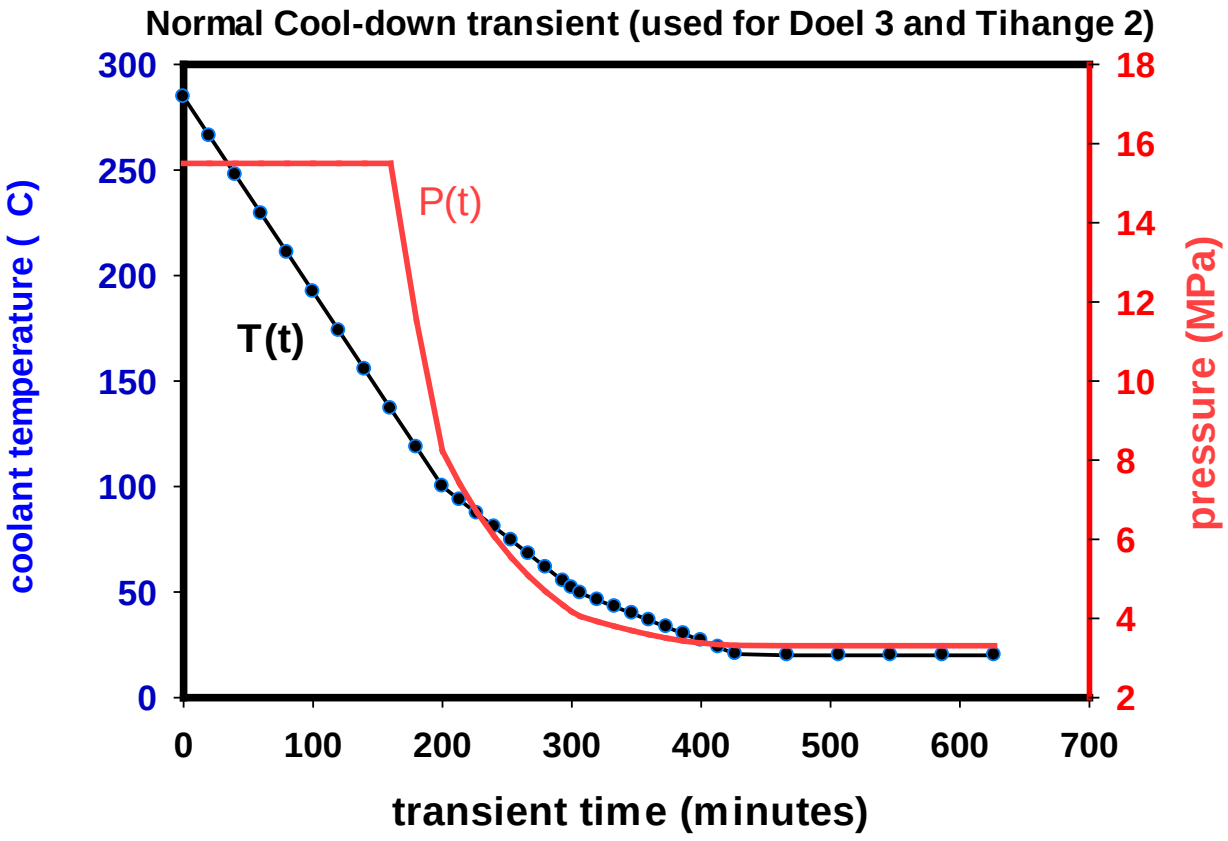

Fig. B.1 Normal cool-down transient used by ORNL for screening assessment of D3/T2.

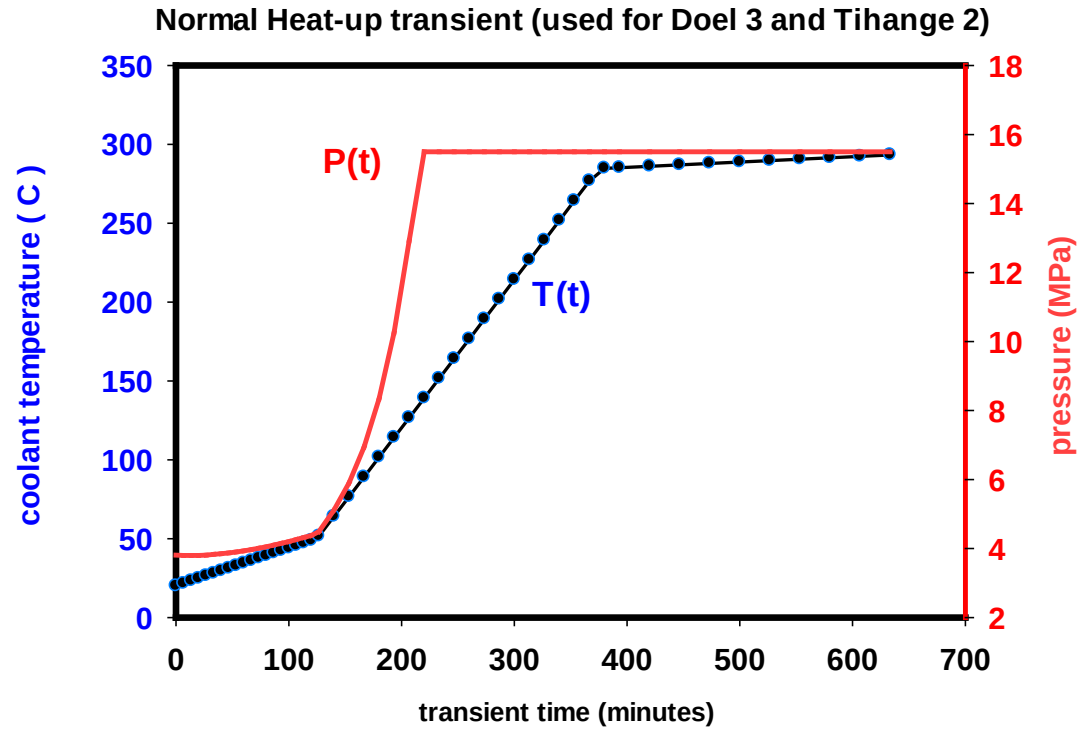

Fig. B.2 Normal heat-up transient used by ORNL for screening assessment of D3/T2.

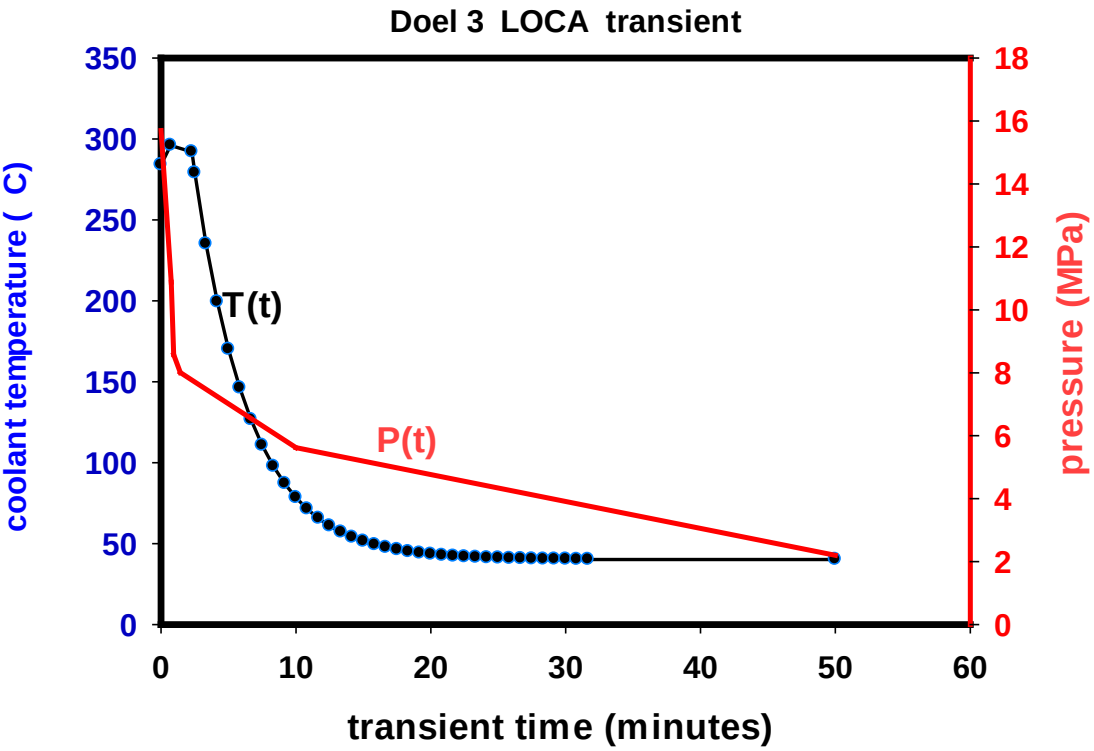

Fig. B.3 LOCA transient used by ORNL for screening assessment of Doel 3 (SLOCA 3 in; SI=40 °C).

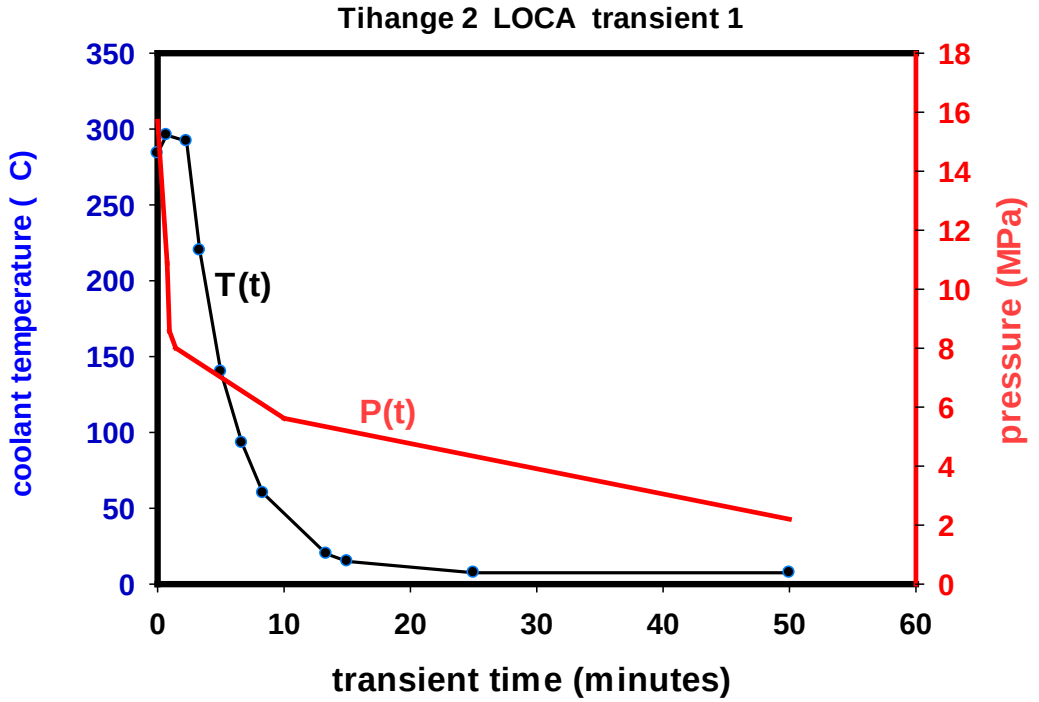

Fig. B.4 LOCA transient used by ORNL for screening assessment of Tihange 2 (SLOCA 3 in; SI=7 °C).

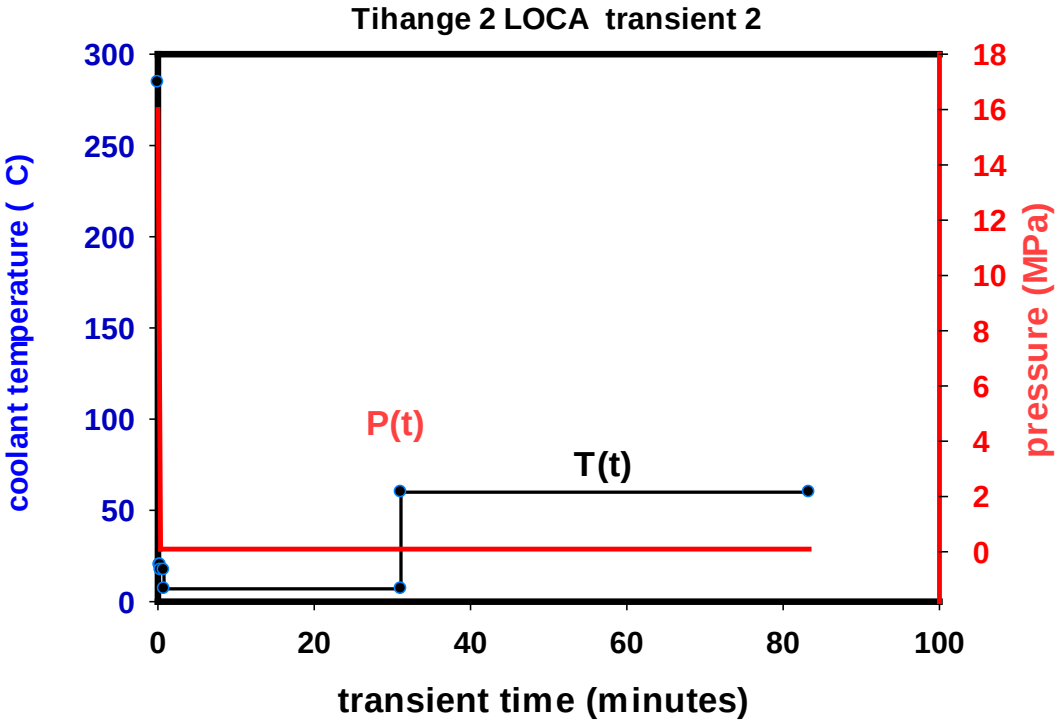

Fig. B.5 LOCA transient used by ORNL for screening assessment of Tihange 2 (LLOCA: SI=7 °C).

APPENDIX B.1 REFERENCES

B.1 Data provided to ORNL - Electrabel Document. September 2015.

APPENDIX C. WARM-PRESTRESS EFFECTS

Appendix C evaluates the effects of invoking warm-prestress (WPS) for those four flaws listed in Table 5.2 (b), *Section* 5.6.5, found not compliant with the ASME acceptance criterion. Inclusion of WPS in the flaw assessment process implies the following [ref. (C.1)]:

- for cleavage fracture to occur at time (t), the applied $K_I(t)$ at the flaw tip
  - must exceed $K_I(t)$ values at all previous times in the transient, and
  - must be greater than or equal to the applicable lower-bound fracture toughness at that location and time (t) in the transient ,
- the last transient time at which $K_I(t)$ exceeds its value for all previous times is the time of maximum (peak) loading, and
- therefore, $RT_{NDT\text{-}CRIT}$ is the minimum RT_{NDT} that provides a point of tangency between the applied $K_I(t)$ at the time of maximum loading and the applicable lower-bound fracture toughness curve.

In the following, the foregoing WPS model implemented in FAVOR is applied in a re-assessment of the four EBL characterized flaws listed in Table 5.2 (b) of *Section* 5.6.5 that are non-compliant according to ASME Section XI (2004).

In Table C.1, the ASME criterion is satisfied if $RT_{NDT\text{-}FINAL} / RT_{NDT\text{-}CRIT} < 1$, where $RT_{NDT\text{-}FINAL}$ is the final "end-of-service-life" value of RT_{NDT} (as specified by EBL) and $RT_{NDT\text{-}CRIT}$ is the minimum value of crack tip RT_{NDT} that creates a point of tangency between the applied $K_I(t)$ and the applicable ASME lower bound fracture toughness curve. This acceptance criterion has no specification of the transient time at which the point of tangency occurs between applied $K_I(t)$ and the fracture toughness curve.

Figure C.1 depicts an assessment of flaw group GP0818 found in the Doel 3 lower shell and subjected to the postulated LOCA (see Appendix B); assessment results are shown with and without inclusion of WPS. Without WPS, a value of $RT_{NDT\text{-}CRIT}$ = 77.9 °C provides a point of tangency between applied $K_I(t)$ and the fracture toughness curve. That point of tangency occurs after the maximum value, $K_{I\max}$, has occurred and, thus, does not satisfy the WPS criteria. Inclusion of WPS increases the critical value to $RT_{NDT\text{-}CRIT}$ = 102 °C. Thus,

- $RT_{NDT\text{-}FINAL} / RT_{NDT\text{-}CRIT}$ = 1.15 without WPS
- $RT_{NDT\text{-}FINAL} / RT_{NDT\text{-}CRIT}$ = 0.88 with WPS

As previously described in Table 5.2 (b), *Section* 5, the flaw group GP0818 in Doel 3 lower shell fails the ASME acceptance criterion; however, invoking WPS renders that flaw group acceptable.

Table C.1 Definition of Parameters Related to Flaw Acceptance Criteria

Parameter	Definition
$\boldsymbol{RT_{NDT\text{-}CRIT}}$	critical value of $\boldsymbol{RT_{NDT}}$ that provides point of tangency between the applied K_I and the applicable ASME lower bound fracture toughness curve
$\boldsymbol{RT_{NDT\text{-}FINAL}}$	"final" $\boldsymbol{RT_{NDT}}$ at "end-of-service-life"
$\boldsymbol{\Delta RT_{MARGIN}}$	$\boldsymbol{(RT_{NDT\text{-}CRIT} - RT_{NDT\text{-}FINAL})}$ margin term used for application of ASME flaw acceptance criterion • $\boldsymbol{\Delta RT_{MARGIN} > 0}$: acceptance criterion is satisfied • $\boldsymbol{\Delta RT_{MARGIN} < 0}$: acceptance criterion is not satisfied
$\boldsymbol{RT_{NDT\text{-}FINAL}/\ RT_{NDT\text{-}CRIT}}$	Alternative parameter for application of ASME flaw acceptance criterion • $\boldsymbol{RT_{NDT\text{-}FINAL}/\ RT_{NDT\text{-}CRIT} < 1}$: acceptance criterion is satisfied • $\boldsymbol{RT_{NDT\text{-}FINAL}/\ RT_{NDT\text{-}CRIT} > 1}$; acceptance criterion is not satisfied

Likewise, Figs. C.2 and C.3 illustrate that two additional EBL-characterized flaws listed in Table 5.2 (b) as non-compliant for Doel 3, i.e., Flaw Group GP0817 and individual flaw 492, respectively, become compliant with application of WPS.

Figure C.4 illustrates that inclusion of WPS in the assessment of individual flaw 1660, found in Tihange 2 and subjected to LOCA 1 (Appendix B), decreases $RT_{NDT\text{-}FINAL} / RT_{NDT\text{-}CRIT}$ from 1.49 to 1.20; thus, flaw 1660 remains non-compliant according to ASME acceptance criterion with or without WPS.

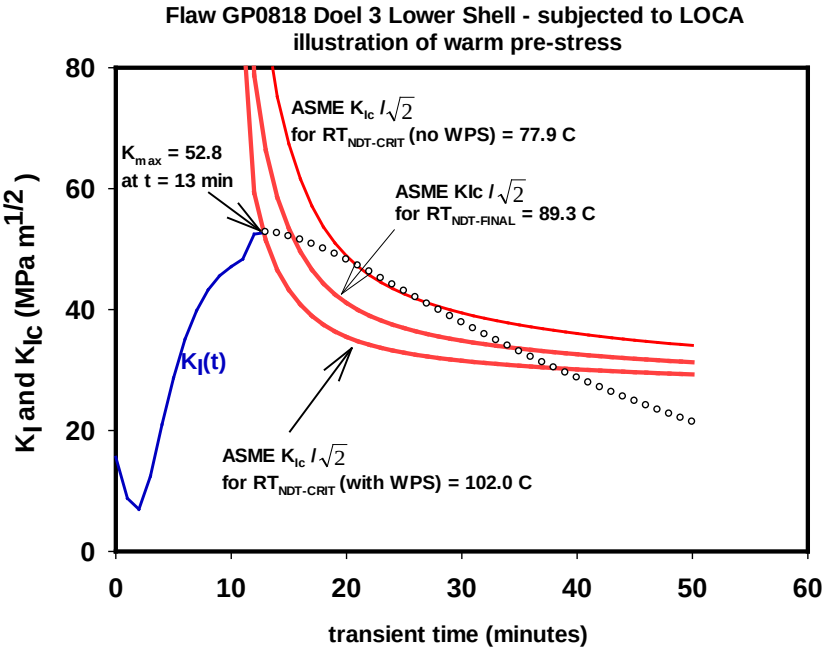

Fig. C.1 Assessment of flaw group GP0818 found in the Doel 3 lower shell and subjected to the postulated LOCA; flaw group passes ASME acceptance criteria if WPS included in the analysis.

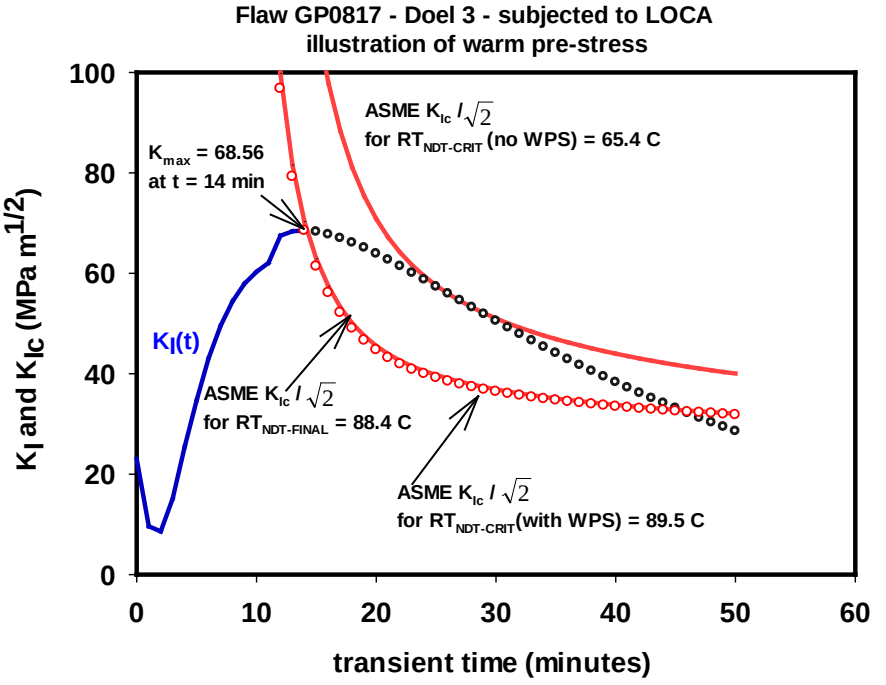

Fig. C.2 Assessment of flaw group GP0817 found in the Doel 3 lower shell and subjected to the postulated LOCA; flaw group passes ASME acceptance criteria if WPS included in the analysis.

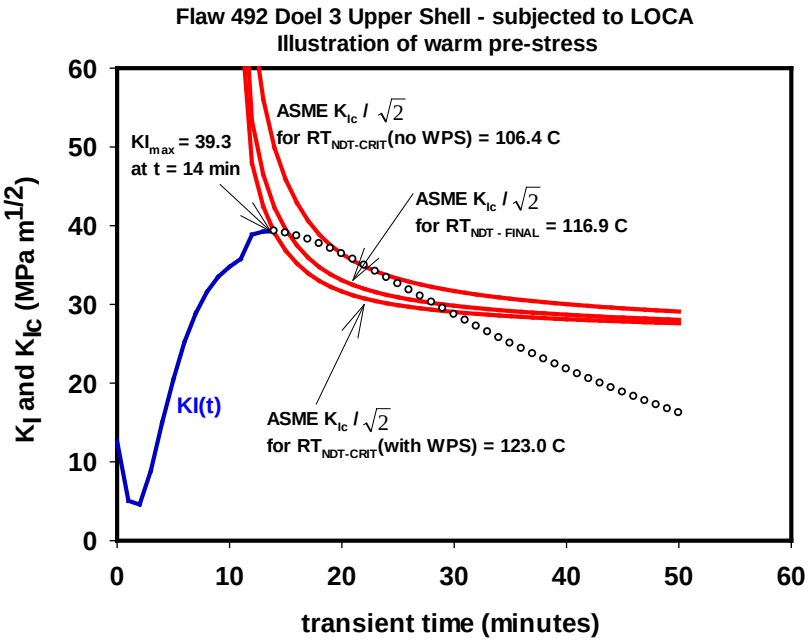

Fig. C.3 Assessment of individual flaw 492 found in the Doel 3 upper shell and subjected to the postulated LOCA; flaw 492 passes ASME acceptance criteria if WPS included in the analysis.

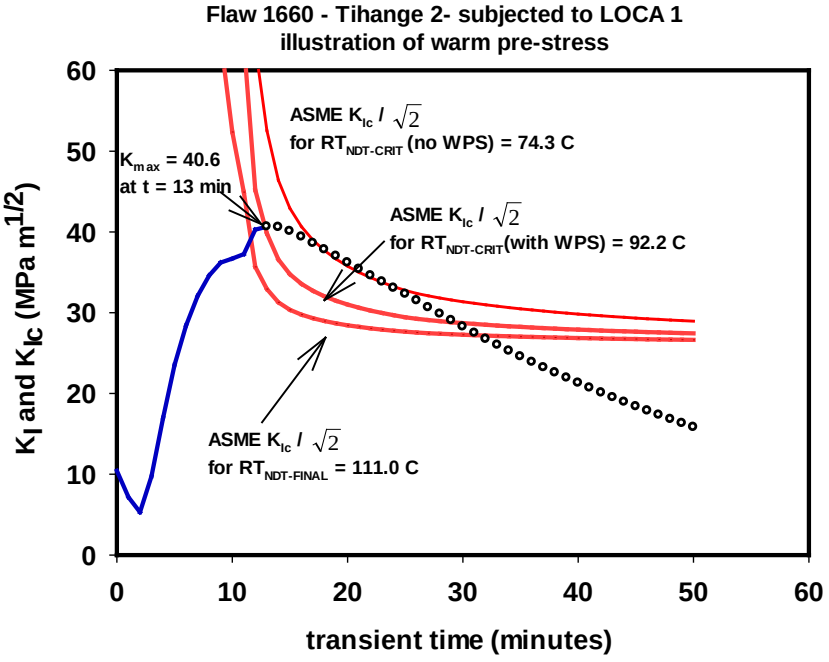

Fig. C.4 Assessment of individual flaw 1660 found in Tihange 2 and subjected to the postulated LOCA 1; flaw is non-compliant according to ASME acceptance criteria with or without WPS.

APPENDIX C.1 REFERENCES

C.1 P.T. Williams, T.L. Dickson, and S. Yin, *Fracture Analysis of Vessels – Oak Ridge FAVOR, v12.1, Computer Code: Theory and Implementation of Algorithms, Methods, and Correlations*, ORNL/TM-2012/567, Oak Ridge National Laboratory, Oak Ridge, TN, November 2012.

APPENDIX D. DETAILS OF ORNL'S REFINED ANALYSIS OF FLAW 1660

Similar to the approach adopted by EBL [D.1, D.2], it was decided to perform a further refined analysis on one of the flaws that did not meet the ASME Section XI acceptance criteria used by ORNL in the SIA of D3/T2. This detailed analysis was carried out using the e**X**tended **F**inite **E**lement **M**ethod (XFEM) capability available in the commercial software program ABAQUS [D.3]. Due to time constraints associated with this review, it was decided to carry out the analysis for one of the individual flaws that failed the acceptance criteria during the SIA using FAVOR. Unlike FAVOR, which is limited to considering elliptical flaws that are oriented along the principal stress axes (i.e., planar flaws), the XFEM approach permits analysis of a flaw with an arbitrary orientation.

Among all the flaws analyzed using FAVOR, the majority of those that did not meet the acceptance criteria were grouped flaws. There were only two individual flaws that failed the acceptance criteria – flaw number 492 from Doel 3 upper shell, and flaw number 1660 from Tihange 2. In order to obtain results in a timely manner, it was decided to limit the refined analysis to one of these two individual flaws. Flaw number 1660 from Tihange 2 was chosen for this purpose, since it had the highest $RT_{NDT\text{-}FINAL}$, and also the largest (negative) ΔRT_{MARGIN} among all the transgressors identified by the FAVOR calculations. In addition, it was the *only* flaw that remained non-compliant if the warm-prestress effect was invoked during the FAVOR analysis (see Appendix C).

For this analysis, the geometry consisted of a section of the cylindrical RPV, as shown in Fig. D.1. The RPV has an inside radius of 1993 mm, clad thickness of 7 mm, and outer radius of 2200 mm. Since the flaw is fairly small in size, it was decided to limit the computational domain to a 4° arc in the circumferential direction of the vessel, and a height of 100 mm in the axial direction. The flaw is almost circular in shape, with major and minor axes of 8.9 mm and 7.9 mm, respectively [D.2]. The flaw was generated by constructing an ellipse with these dimensions in the YZ-plane, and then by tilting it by 20° about the Y-axis (parallel to the circumferential direction), and by 19.3° about the Z-axis (axial direction). The bounding box for this flaw had a depth in the radial direction of 2.95 mm, and a ligament (distance of the edge closest to the vessel inner diameter from the clad-base metal interface) of 1.14 mm. In order to locate the flaw at the center of its bounding box, it was placed in the domain at a distance of 2.615 mm from the clad-base interface. The mesh for the XFEM analysis was generated with higher mesh refinement in the vicinity of the flaw as shown in Figs. D.2 (overall view) and D.3 (close up view in the vicinity of the flaw). The mesh for both the thermal and mechanical analyses was generated using 8-node linear hexahedral elements, with close to 290,000 elements over the entire domain.

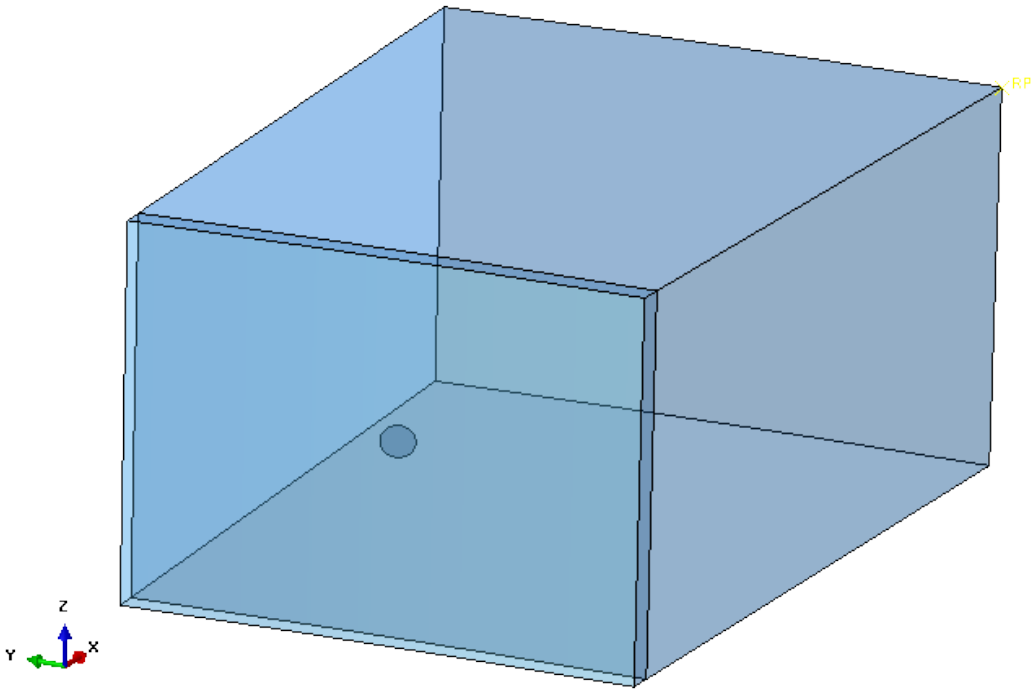

Fig. D.1 Section of Tihange 2 RPV used for analysis of the flaw number 1660 using XFEM.

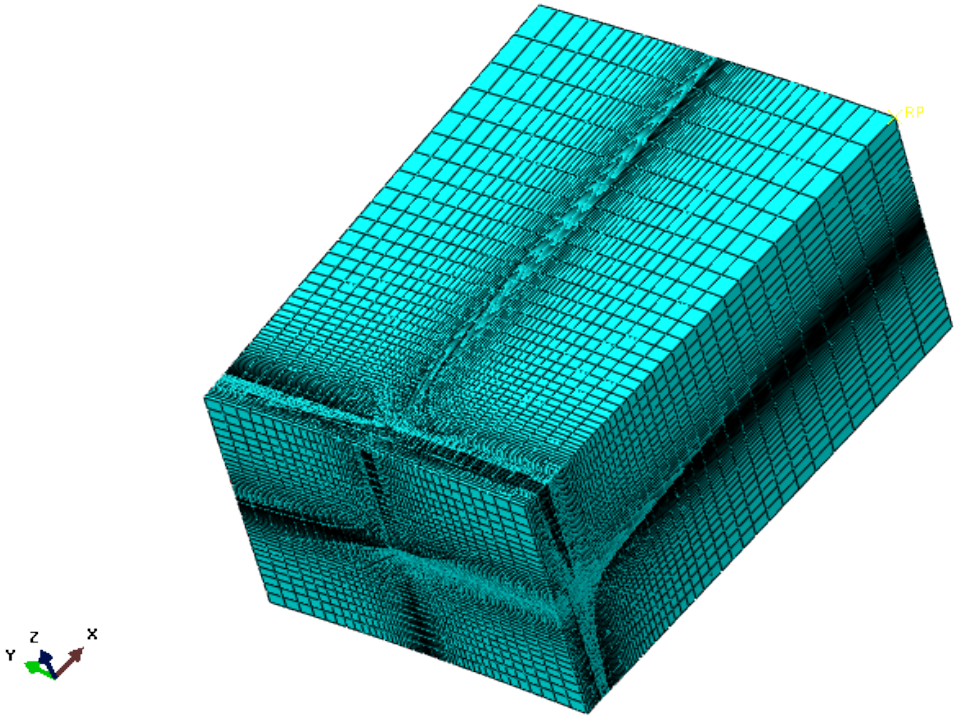

Fig. D.2 Mesh used for the analysis of flaw number 1660 (overall view).

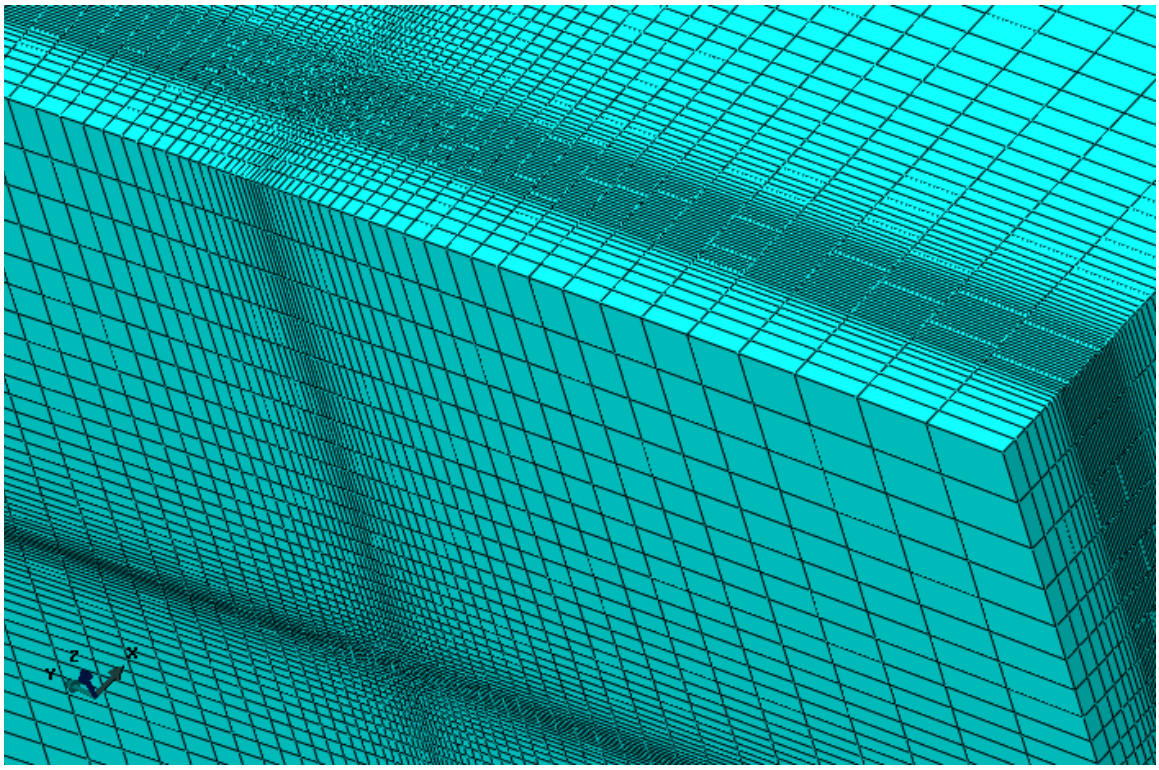

Fig. D.3 Mesh used for the analysis of flaw number 1660 (close up view in the vicinity of the flaw).

The analysis was performed in two stages. The first step involved a thermal analysis to compute the temperature field over the domain and its evolution with time. The conditions for the small break LOCA transient were used for this analysis [D.4]. The variation with time of the coolant temperature and the heat transfer coefficient were prescribed at the clad inside surface, and all other surfaces were assumed to be insulated. The results of the thermal analysis were then provided as input for the subsequent mechanical analysis.

For the mechanical analysis, the inside surface of the vessel was subjected to internal pressure, which also varied with time [D.4]. The effect of the internal pressure acting on the top surface of the vessel was taken into account by prescribing a concentrated load at one of the nodes on the top surface of the model. This load was scaled to account for the reduction in the circumferential dimension of the model compared to the full cylinder of the RPV wall. The bottom surface in the axial direction and the two surfaces with a normal in the circumferential direction were subjected to symmetry boundary conditions. The top surface in the axial direction was constrained to remain planar, by requiring all nodes on the top surface to have the same displacement in the axial direction.

In addition to the analysis of the tilted flaw number 1660, the same model geometry was also used to analyze the two resolved elliptical flaws, one in the axial and other in the circumferential direction, that were generated for the SIA using FAVOR (see Fig. 5.7, *Section 5.6.2*). These flaws had an aspect ratio of 3, and they were positioned such that their center was at the same location as that of the tilted flaw, as shown in Fig. D.4. The simulations using the resolved flaws in the axial and circumferential directions were carried out for the purpose of comparing the results of the XFEM analyses against the results obtained from FAVOR.

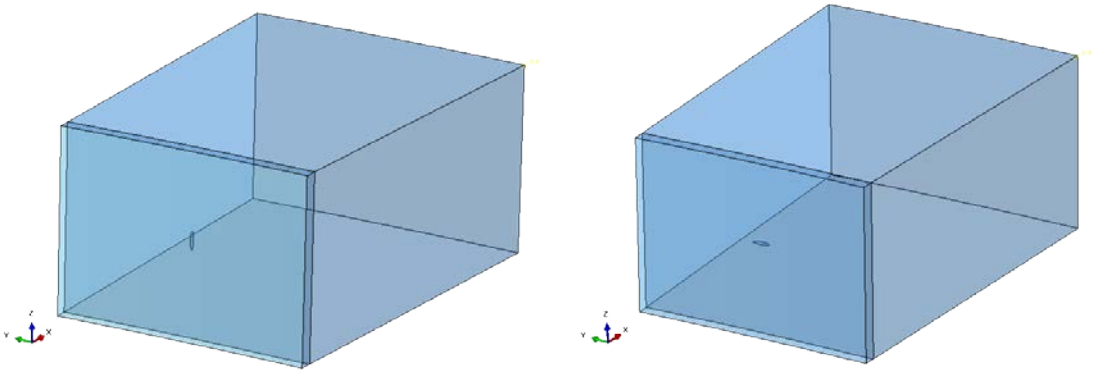

Fig. D.4 Section of Tihange 2 RPV showing the resolved axial flaw (left) and circumferential flaw (right) used in the XFEM analysis.

Figure D.5 compares the variation of the applied K_I with time from the ABAQUS XFEM and FAVOR simulation results for the axial and circumferential flaws at the inner crack tip (location closest to the vessel inner diameter), showing good agreement between the two approaches. Figure D.6 shows the results for the variation of the applied K_I with time calculated using ABAQUS XFEM for the quasi-laminar flaw number 1660, and how this compares with similar calculations for the two resolved flaws. Following the approach used by EBL for mixed-mode loading of the Q-L flaw (assuming a plane strain stress-strain state), an equivalent K_I value can be calculated using the following expression.

$$K_{eq} = \sqrt{K_I^2 + K_{II}^2 + \frac{1}{1-\nu} K_{III}^2} \qquad \text{(D.1)}$$

The stress-intensity factor, K_{eq}, in Eq. (D.1) corresponds to an combined energy release rate, G_{eq}, for a mixed-mode multi-axial loading condition that includes contributions to G from three crack-tip loading/deformation modes, Modes I, II, and III.[7] These contributions are additive (see Eq. (2.63) in Ref. [D.5]) resulting in the equation given above for a state of plane strain. It is clear from Fig. D.6 that the actual flaw orientation for 1660 leads to a much lower K_I value compared to the two resolved flaws. Also plotted in Fig. D.6 is the K_{Ic} lower bound fracture toughness curve with a safety factor of $\sqrt{2}$, corresponding to the $RT_{NDT\text{-}FINAL}$ of 111 °C for flaw number 1660, and it lies well above the K_I curve for the quasi-laminar flaw. The highest value of the applied K_I for the quasi-laminar flaw is 20.7 MPa$\sqrt{}$m, and this value compares fairly well with the 21.7 MPa$\sqrt{}$m reported by EBL [D.2]. The highest value is also lower than the $K_{IC}/\sqrt{2}$ lower shelf value of 23.48 MPa$\sqrt{}$m, indicating that there is no critical RT_{NDT} for this flaw. It should be noted that the XFEM analysis reported here was based on linear elastic fracture mechanics, whereas the EBL refined analysis for flaw number 1660 used an elastic-plastic calculation due to proximity of the flaw to the clad-base metal interface. The current XFEM implementation in ABAQUS, v6.14-1, is limited to linear-elastic materials and, therefore, limited to LEFM analyses.

[7] Mode I fracture is an *opening* mode with a tensile stress applied normal to the crack plane. Mode II fracture is a *sliding* mode with an in-plane shear stress applied parallel to the crack plane and normal to the crack front. Mode III fracture is a *tearing* mode with an out-of-plane shear stress applied parallel to the crack plane and parallel to the crack front.

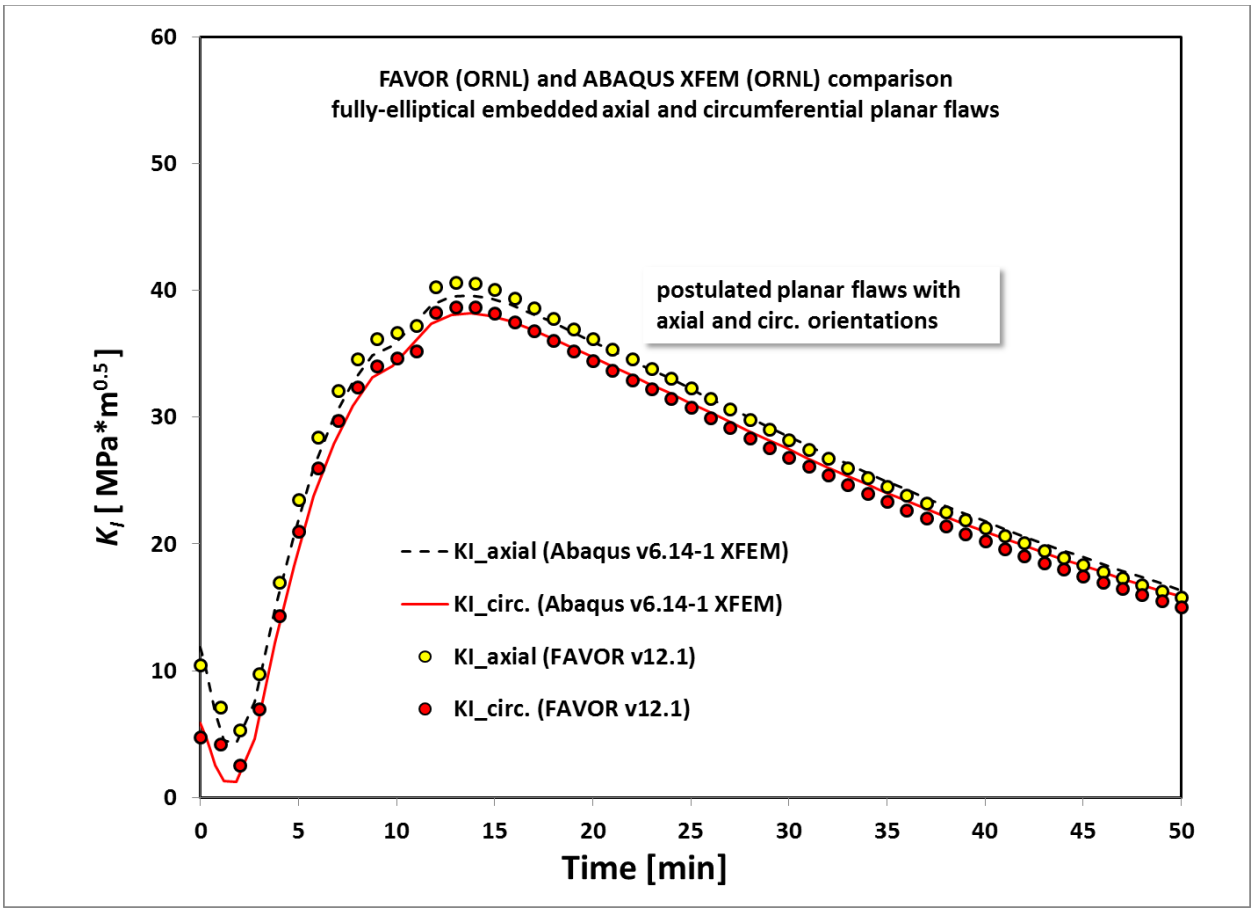

Fig. D.5 Variation of applied K_I with time at the inner crack tip for the resolved axial and circumferential flaws based on FAVOR and ABAQUS XFEM simulations.

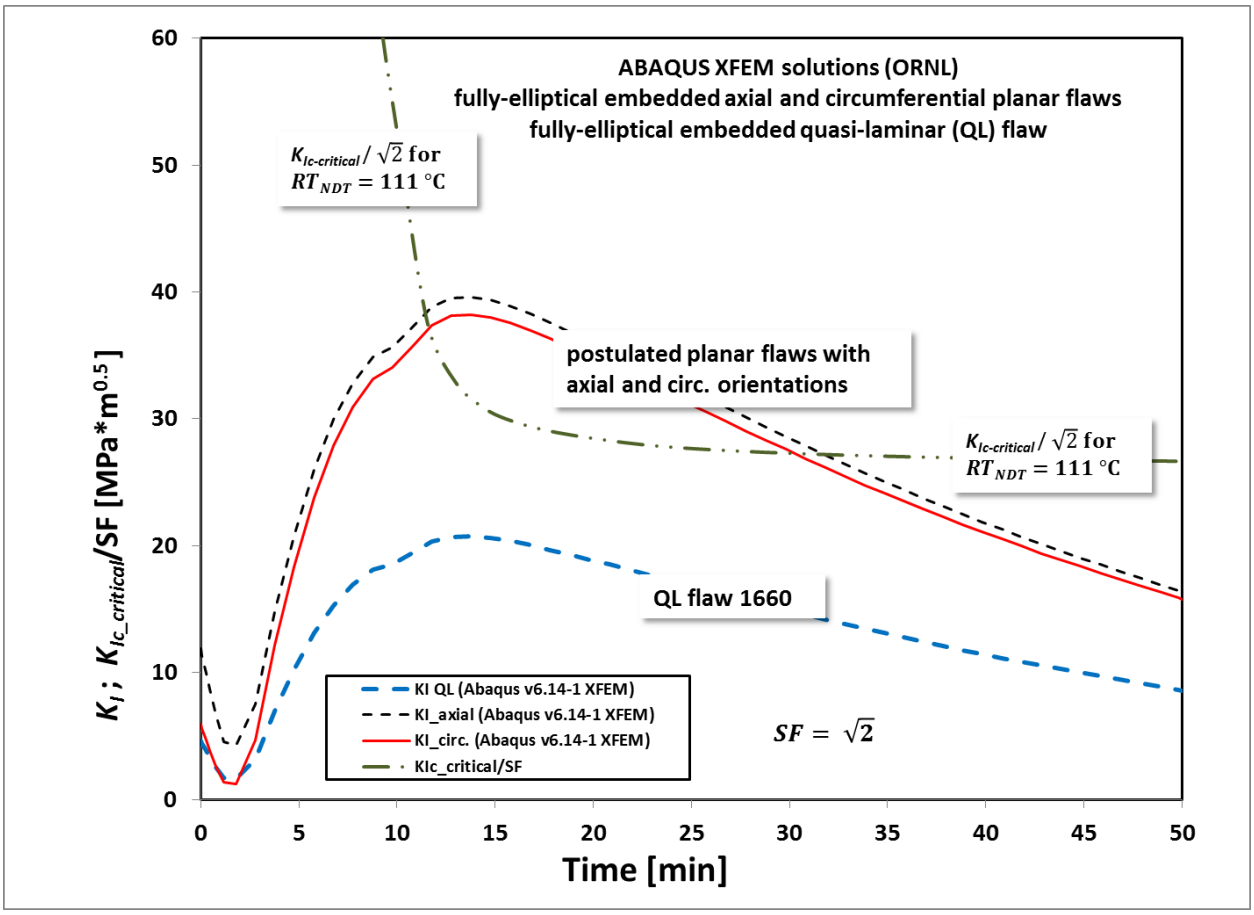

Fig. D.6 Variation of applied K_I with time for the quasi-laminar flaw, and for the resolved axial and circumferential flaws, based on the ABAQUS XFEM simulations.

APPENDIX D.1 REFERENCES

D.1 4.4.2 – Calculations: RPV Doel 3: 3-D multi-flaws and refined analyses. Tractebel Engineering Report CNT-KCD/4NT/0018107/000/02, (2014).

D.2 4.4.2 – Calculations: RPV Tihange 2: 3-D multi-flaws and refined analyses. Tractebel Engineering Report CNT-KCD/4NT/0021061/000/00, (2014).

D.3 ABAQUS Finite Element Software, Version 6.14-1 (Standard), Dassault Systems Simulia Corp., Providence, RI (2014).

D.4 Data provided to ORNL. Electrabel Document. September 2015.

D.5 T.L. Anderson, *Fracture Mechanics – Fundamentals and Applications*, 3rd ed., Taylor and Francis, Boca Raton, FL (2005).